**Title**
Studies of the Hydraulic Behavior of Hierarchically Fractured Rock Geometries



**Author**
Polek, J.M.

**Publication Date**
1990-02-01

Lawrence Berkeley Laboratory
UNIVERSITY OF CALIFORNIA

EARTH SCIENCES DIVISION

# Studies of the Hydraulic Behavior of Hierarchically Fractured Rock Geometries

J.M. Polek
(M.S. Thesis)

February 1990



**Prepared for the U.S. Department of Energy under Contract Number DE-AC03-76SF00098.**

## DISCLAIMER

LBL-28612

# Studies of the Hydraulic Behavior of Hierarchically Fractured Rock Geometries

**James M. Polek**

(M.S. Thesis)

Earth Sciences Division
Lawrence Berkeley Laboratory
University of California
Berkeley, California 94720

February 1990

This work was supported by the U.S. Department of Energy under Contract No. DE-AC03-76SF00098.

# Table of Contents

List of Figures ..... v

List of Tables ..... vii

Acknowledgements ..... viii

CHAPTER 1 INTRODUCTION ..... 1

CHAPTER 2 BACKGROUND ..... 3

2.1. Introduction ..... 3

2.2. Fractured Rock Models ..... 3

2.3. Fractal Rock Geometries ..... 6

CHAPTER 3 CODE DESCRIPTION ..... 8

3.1. Introduction ..... 8

3.2. FMG ..... 8

3.3. RENUM ..... 9

3.4. LINEL ..... 10

3.5. ELLFMG ..... 11

3.6. DIMES and ELLP ..... 12

3.7. TRINET ..... 12

3.8. PT ..... 13

3.9. FMMG ..... 13

CHAPTER 4 HIERARCHICALLY FRACTURED SYSTEMS ..... 16

4.1. Introduction ..... 16

4.2. FMMG Mesh Validation ..... 16

4.3. Numerical Study ..... 19

4.3.1. Mesh Geometry ..... 19

4.3.2. Procedure ..... 23

4.3.3. Results ..... 23
4.4. Equivalent Porous Media ..... 25
4.4.1. Steady State Conditions ..... 27
4.4.2. Transient Conditions ..... 28
4.5. Conclusions ..... 31

CHAPTER 5 FRACTAL ROCK SYSTEMS ..... 33
5.1. Introduction ..... 33
5.2. Background ..... 34
5.2.1. Percolation Theory ..... 35
5.2.2. Sierpinski Carpet ..... 37
5.3. Percolating Network ..... 39
5.4. Modified Sierpinski Carpet ..... 41
5.5. Fractal Dimension ..... 45
5.6. Radial Fractal Dimension ..... 49
5.7. Flow Equation Solution ..... 53
5.8. Results ..... 59
5.9. Conclusions ..... 64

CHAPTER 6 CONCLUSIONS AND FUTURE STUDIES ..... 66

REFERENCES ..... 70

# LIST OF FIGURES


| | | |
|---|---|---|
| Figure 3.1 | Fracture-matrix mesh. | 15 |
| Figure 4.1 | (a) Control mesh. (b) Second mesh, with random fractures. (c) Third mesh, with discretized matrix. | 18 |
| Figure 4.2 | Pressure response curves of three different mesh geometries. | 20 |
| Figure 4.3 | Negative exponential distribution and the generated fracture sets. | 22 |
| Figure 4.4 | Fracture meshes with decreasing number of sets from (a) to (h). | 24 |
| Figure 4.5 | Permeability vs. truncation length with (a) constant aperture, (b) distributed aperture, (c) correlated aperture. | 26 |
| Figure 4.6 | (a) Mesh with all the fractures. (b) Mesh with small fractures replaced by blocks of porous media. | 29 |
| Figure 4.7 | Transient pressure response curves at Node A and B in the fracture only mesh and Node A' and B' in the fracture porous media mesh. | 30 |
| Figure 5.1 | (a) Square lattice. (b) Percolation clusters. | 36 |
| Figure 5.2 | Sierpinski carpet for $N = 8$ (a) carpet initiator, (b) carpet generator, and (c)-(e) carpet construction stages. | 40 |
| Figure 5.3 | Backbone cluster of percolating network. | 40 |
| Figure 5.4 | Percolating networks that are 64 unit length fractures across (a) $p = 0.3473$, (b) $p = 0.3450$, (c) $p = 0.3500$, and (d) $p = 0.4000$. | 42 |
| Figure 5.5 | Percolating networks that are 243 unit length fractures across (a) $p = 0.3473$, (b) $p = 0.3450$, (c) $p = 0.3500$, and (d) $p = 0.3800$. | 43 |
| Figure 5.6 | Modified Sierpinski carpets for $N = 5$ (a) carpet initiator, (b) carpet generator, and (c)-(e) carpet construction stages. | 44 |

| | | |
|---|---|---|
| Figure 5.7 | Modified Sierpinski carpet for $N = 6$ and with the fractures placed at random. | 46 |
| Figure 5.8 | Modified Sierpinski carpets with fractures placed at random (a) $N = 3$, (b) $N = 4$, (c) $N = 5$, and (d) $N = 6$. | 47 |
| Figure 5.9 | Fracture density plots of the size 64 percolating networks (a) $p = 0.3473$, $D = 1.2$ (b) $p = 0.3450$, $D = 1.3$ (c) $p = 0.3500$, $D = 1.4$ (d) $p = 0.4000$, $D = 1.8$. | 50 |
| Figure 5.10 | Fracture density plots of the size 243 percolating networks (a) $p = 0.3473$, $D = 1.3$ (b) $p = 0.3450$, $D = 1.5$ (c) $p = 0.3500$, $D = 1.7$ (d) $p = 0.3800$, $D = 1.7$. | 51 |
| Figure 5.11 | Fracture density plots of the modified Sierpinski carpets (a) $N = 3$, $D = 1.2$ (b) $N = 4$, $D = 1.4$ (c) $N = 5$, $D = 1.5$ (d) $N = 6$, $D = 1.6$. | 52 |
| Figure 5.12 | Radial fracture density plots of the size 64 percolating networks (a) $p = 0.3473$, $D = 1.1$ (b) $p = 0.3450$, $D = 1.3$ (c) $p = 0.3500$, $D = 1.3$ (d) $p = 0.4000$, $D = 1.6$. | 54 |
| Figure 5.13 | Radial fracture density plots of the size 243 percolating networks (a) $p = 0.3473$, $D = 1.3$ (b) $p = 0.3450$, $D = 1.4$ (c) $p = 0.3500$, $D = 1.7$ (d) $p = 0.3800$ $D = 1.7$. | 55 |
| Figure 5.14 | Radial fracture density plots of the modified Sierpinski carpets (a) $N = 3$, $D = 1.2$ (b) $N = 4$, $D = 1.4$ (c) $N = 5$, $D = 1.5$ (d) $N = 6$, $D = 1.6$. | 56 |
| Figure 5.15 | Incomplete gamma function (Barker 1988). | 58 |
| Figure 5.16 | Pressure response curves of the size 64 percolating networks (a) $p = 0.3473$, (b) $p = 0.3450$, (c) $p = 0.3500$, (d) $p = 0.4000$. | 60 |
| Figure 5.17 | Pressure response curves of the size 243 percolating networks (a) $p = 0.3473$, (b) $p = 0.3450$, (c) $p = 0.3500$, (d) $p = 0.3800$. | 61 |
| Figure 5.18 | Pressure response curves of the modified Sierpinski carpets (a) $N = 3$, (b) $N = 4$, (c) $N = 5$, (d) $N = 6$. | 62 |

# LIST OF TABLES


| | | |
|---|---|---|
| Table 4.1 | Fracture length and density distribution | 22 |
| Table 5.1 | Geometric and flow dimensions of the size 64 percolating networks. | 63 |
| Table 5.2 | Geometric and flow dimensions of the size 243 percolating networks. | 63 |
| Table 5.3 | Geometric and flow dimensions of the modified Sierpinski carpets. | 63 |

# ACKNOWLEDGEMENTS

I would first like to thank Professor Paul Witherspoon for introducing me to the field of hydrogeology and for his support and guidance throughout my years as a graduate student. It has been a priviledge to work under him. I would like to extend my thanks to Dr. Jane Long for her direction and support while working with her, and for her help with my thesis. In addition, my thanks to Professor Malcolm McPherson for his guidance and encouragement during my years at Cal.

I want to express my sincere thanks to Kenzi Karasaki for the invaluble help he has given me. If it were not for Kenzi's motivation and enthusiasm, this research would never have been initiated. I have truly enjoyed working with Kenzi and have learned a great deal from him.

I want to thank Kurt Nihei for his help with the computer. Many frustrating hours were avoided by listening to his thoughtful suggestions. I want to extend a special thanks to Professor Neville Cook for the direction and help he has given me over the years.

I would like to thank my parents, Tom and Susie, for the support and encouragement they have given me my entire life. They taught me how to be hard working and fun loving, two traits that got me through my college years.

Lastly, and most importantly, I want to thank my wife, Anna-Marie, who brings out the best in me. Anna-Marie motivated me to go to graduate school and her love and support helped me through it.

# CHAPTER 1

# INTRODUCTION

The hydraulic behavior of fractured rock is of special interest to workers in such areas as oil recovery, geothermal energy, toxic and hazardous waste disposal, groundwater contamination and nuclear waste storage. The fractures within a rock may constitute a large amount of the rock's void space and in many situations will comprise the primary conduit for flow through the rock.

The studies of flow through fractured rock are usually performed in field tests, laboratory experiments or numerical simulations. There are advantages and disadvantages to each of these methods. Field tests can be expensive, time consuming and in many instances impractical to carry out. They have the advantage of producing results that are representive of the area. Laboratory experiments on rock samples produce data that is representative of the sample, but problems may occur in extrapolating the data to larger areas of interest. The sample size would be dictated by the equipment and space available. Numerical modeling can be done on a wide range of scales but there may be difficulty in relating the numerical data to the field. The emphasis of this work is the study of the hydraulic behavior of various rock geometries which lends itself best to numerical modeling. Different fracture geometries are best studied using numerical modeling, since the geometries can be created prior to the flow simulations. For both field and laboratory tests the geometry of the rock's fracture pattern is not usually known.

Throughout this paper, the term "fracture" is used as an all encompassing term for rock discontinuities, such as joints, fissures, faults and microfractures. Fractures over a range of length scales were used in the flow simulations in order to obtain realistic flow characteristics of fractured rock. The flow simulations

have been broken up into two studies. The first of these studies is presented in Chapter 4 and concerns the effects of fracture length and aperture on the permeabilities of rock systems. Simplifications to fracture geometries were made to examine the possiblilty of creating systems with equivalent flow characteristics. By simplifying the rock systems the amount of computer memory and usage could be decreased, which would result in faster and less expensive flow simulations of fractured rock. The rock systems used for this study are hierarchically fractured, that is the fractures are assigned to specific sets designated by their fracture length. The number of fracture sets used in each flow simulation is varied and the possibility of replacing the smaller fractures with an equivalent porous media is studied.

The second study is presented in Chapter 5 and investigates the use of fractal geometry to represent the geometry of fractures. Two different fractal geometries are used to study the dependence of the flowing fluid on the geometry of the fracture system. A non-Euclidean dimension, called the flow dimension, is presented to describe the flow through fractured rock systems during simulated well tests. The flow dimensions are compared to the fractal dimensions of the rock systems. It may be possible to calculate the flow dimension from field well tests which may lead to a way of describing the rock geometry surrounding the well (Barker 1988).

The flow simulations conducted in these studies were accomplished by using a number of computer codes. The function of each of these codes will be described in Chapter 3. The background of modeling fractured rock will be presented in the following chapter.

# CHAPTER 2

# BACKGROUND

## 2.1. Introduction

Fluid flow through fractured rocks, especially low permeability crystalline rocks, may be dominated by the fractures due to their high conductivity to fluids. Between these fractures lies intact rock, referred to as the rock matrix. The geometries of the fractures and intact rock are generally unknown and very complex. Some of this complexity stems from the fact that fractures exist at all length scales. Fractures can range from kilometers in length down to the length of a rock grain. Since the entire spectrum of fracture lengths cannot be considered when solving fluid flow through fractured rock, some simplifications must be made.

## 2.2. Fractured Rock Models

One of the first simplifications made when modeling fractures is that a fracture can be represented by the space between two smooth parallel plates. The flowrate through the idealized fracture described above is given by:

$$Q = \frac{b^3 \rho g}{12\mu} \left[\frac{dh}{dx}\right] w \tag{2.1}$$

where:

$Q$ = Volumetric flowrate ($m^3/s$)

$b$ = Fracture aperture ($m$)

$\rho$ = Fluid density ($kg/m^3$)

$g$ = Acceleration due to gravity ($m/s^2$)

$\mu$ = Fluid viscosity ($kg/s-m$)

$h$ = Hydraulic head ($m$)

$x$ = Flow path length ($m$)

$w$ = Width of fracture ($m$)

This equation is commonly called the cubic law since the flowrate is a function of the aperture cubed. The fracture permeability, $k_f$, is defined to be $b^2/12$ and has the units of ($m^2$). The hydraulic conductivity of the fracture, $K_f$, is defined to be $k_f \rho g / \mu$ and has the units of ($m/s$). Throughout this paper the term "permeability" is used for both permeability and hydraulic conductivity, and a differentiation can be made by checking the units with which the values are expressed. The cubic law has been used by many to describe flow in smooth walled fractures. It has been extended to rough walled fractures by multiplying by a factor to describe the roughness of the fractures surface (Witherspoon et al. 1980). Much work has been done on the study of single fractures, but the emphasis of this paper is to model fractured rock using a great number of fractures.

A method for modeling fractured rock was introduced by Snow (1965, 1969). He considered the fractures to be infinite in extent and replaced them with a porous media that had a permeability tensor calculated from the individual fracture permeabilities. The individual fracture permeabilites were calculated from the cubic law. He studied the effect on permeability of varying the fracture orientation and aperture. One of the limitations of his approach was the assumption that the fractures were considered to be infinite in extent which is not true in fractured rock.

The double porosity model, introduced by Barenblatt, Zheltov, and Kochina (1960), and later extended by Warren and Root (1963), also makes the assumption that the fractures are infinite in extent. This mathematical model does, however, take the matrix rock into account. The matrix is assumed to have a high

storage capacity and low permeability with respect to the fractures. Given these conditions, the fractures and the matrix can each be represented by an equivalent porous media. The porosity of the porous media representing the fractures will be smaller than the porosity of the porous media representing the matrix . The matrix porous media only acts as a source of fluid for the fracture porous media and is not considered to contribute to the flow characteristics of the overall system. In the original double porosity models the flux between the fractures and matrix was considered to be at a pseudo-steadystate, so the quantity of flux was proportional to the pressure difference at the fracture-matrix interface. The pressure gradient within the matrix was considered to be linearly distributed. Later work by Kazemi (1969), de Swaan (1976), Streltsova (1983) and Lai (1985) assumed that the flux at the fracture-matrix interface was transient and the pressure gradient within the matrix was not distributed linearly. This transient flow in the matrix changes the shape of the pressure response curve during the transient flow period.

The previous models all assume that the fractures are infinite in extent. A model was developed by Baecher et al. (1977) and Barton (1978) that allow for fractures of finite length. In three dimensions the fractures appear as elliptical disks and in two dimensions as lines. Any sized fracture length, aperture or orientation can be chosen. The fracture length and spacing distributions have been studied by Hudson and Priest (1979) and Baecher and Lanney (1978) and have been found to vary both log normally and exponentially. Using these distributions and the fracture model descibed above, Long et al. (1982) developed a computer code to construct two dimensional fractured rock systems which solved the permeabilties of these systems. This code was used to study the effects of discontinuous fractures on the system's permeability as well as the possibility of replacing discontinuous fracture systems with an equivalent porous media. The effects of

fracture interconnection on permeabilty were also studied (Long and Witherspoon 1985). The code was extended to three dimensional systems by Gilmour et al. (1986). Karasaki (1987) extended the modeling of two dimensional fracture systems by modeling the matrix rock in addition to the fractures. Explicit modeling of fractures and matrix dispenses with the assumptions made in the double porosity model that the fractures behave as an equivalent continuum and that the through-flow in the matrix is negligible (Karasaki 1987).

The work presented in Chapter 4 uses both the Long and the Karasaki models to study the effects of fracture length and orientation on the permeability of two dimensional rock systems.

## 2.3. Fractal Rock Geometries

Another approach to modeling fractured rock is to use fractals to represent the fractures. A fractal is a shape, comprised of parts, that looks similar at all scales. A fractal structure seems to be random and complex, just as the geometry of fractures is random and complex. The fractal structure, however, can be described by a number called the fractal dimension. The fractal dimension has been defined by many (Mandelbrot 1982, Feder 1988 and Stauffer 1985). A definition of the fractal dimension is presented in Chapter 5.

The use of fractal geometry to describe rock has been small and has been mostly limited to modeling porous media rather than fractured rock. Using a model of porous media that had a fractal structure, Alder (1985) found that the fractal porous media was a better model of real porous media than was a spacially periodic model. Hewett (1986) found that fractal distributions showed promise for assessing the flow characteristics of heterogeneous porous media. It was shown by Chen and Wilkinson (1985) and Maloy et al. (1986) that the flow paths of a highly viscous fluid in a saturated random porous media formed fractal structures.

Oxaal et al. (1987) demonstrated that the flow within these viscous fluid flow paths was also fractal. The fractal dimension of the flowing fluid, however, was less than the fractal dimension of the original flow paths. This implies that the flowing fluid prefers some paths over others and that it only uses a fraction of the original flow paths. A "statistical factor" involving gas flow through percolating clusters of rock cracks was introduced by Englman (1983) to account for the fact that the flow does not pass through every fracture. Although he postulated the existence of this factor, no further work was done to derive it.

Fractal geometry was used by Nolte et al. (1987) to study the flow paths in natural fractures. They found that the flow path area of a natural fracture was fractal. The fractal dimension was dependent on the stress applied to the fracture. The fractal behavior of rock is not limited to single fractures but has been observed in naturally fractured rock. Barton (1987) found from his pavement studies that the fracture trace length distributions had fractal characteristics. Since natural fractures exhibit fractal properties, it seems reasonable to use fractal geometries to model rock fractures. Two different fractal geometries are used to model fractured rock and are presented in Chapter 5. Fluid flow through these fractal rock systems will be analyzed in order to understand the flow's dependence on the fracture geometry.

# CHAPTER 3

# CODE DESCRIPTION

## 3.1. Introduction

The programs that are described in the following sections were used to model flow through fractured rock systems for the studies presented in this paper. The programs are executed in a certain order depending on which fracture system is being studied. For a system containing only fractures, having no porous matrix, the series of programs executed starts with FMG. RENUM is run next and is followed by DIMES if a graphic representation of the system is desired. The next program to be executed is LINEL, if steady state flow conditions are desired, or TRINET, if transient flow conditions are desired. If steady state flow conditions are being studied then ELLFMG can be run following LINEL. ELLP can be executed after ELLFMG to give a graphic representation of the permeability ellipse calculated in ELLFMG (see Section 3.5).

To study rock systems containing both fractures and porous matrix the FMMG program should be executed between FMG and RENUM, and PT should be executed rather than LINEL or TRINET.

## 3.2. FMG

The fracture mesh generator, FMG (Long et al 1982), creates a two dimentional numerical representation of fractured rock, called a fracture mesh. The fractures of the mesh are represented by line segments. Input to FMG contains information about the size, the boundary conditions and the fracture characteristics of the mesh, such as length, orientation, aperture and density.

The dimensions of the mesh, given in the input deck, define the size of

the generation region. A subset of the generation region is the flow region. The flow region is smaller than or equal to the generation region and its dimensions are also given in the input deck. The flow region is the area of the mesh where flow is calculated.

The boundary conditions of the flow region are input to FMG and are necessary for flow tests. The possible boundary conditions for this program are; constant flux, no flow, constant head, or constant linearly distributed head.

The fracture characteristics given in the input deck include the fracture density, length, orientation and aperture. The fracture density can be given as a number of fractures per unit area of the generation region or as a total number of fractures within the generation region. The values for the fracture length, orientation and aperture can each be set at a constant value, they can be assigned specific values or they can be statistically generated. Some possible statistical distributions are normal, uniform, lognormal and negative exponential. A random seed generator is used when calculating values from these statistical distributions.

Once the input deck is created, the FMG program can be executed. The output from the FMG program will be the necessary input for the remaining programs that are executed.

### 3.3. RENUM

The RENUM program (Billaux et al. 1988) will use an output file from FMG for its input. The file contains the information about the structure of the mesh generated by FMG. The fractures in the mesh are described by nodes and elements. Nodes are located at the ends of fractures and at intersections of fractures. Elements are line segments that connect two nodes. All of the nodes and elements are numbered and put into two separate lists.

RENUM reads the input file which contains the list of node numbers,

their location designated by x and y coordinates. The file also specifies on which boundary, if any, the nodes lie. Next in the file is the list of all the elements. Listed for each element are the element number, the two nodes the element connects, the transmissivity of the element, and the length of the element.

The purpose of RENUM is to optimize node numbering for flow calculations and to check the structure of the mesh and remove any potential problems. The RENUM program looks for nodes that are very close to one another and combines them into one node as well as eleminating any zero length elements that may have been created. The program also follows the path of fractures connected to a boundary and, in the event that the path closes on the same boundary, the path is deleted. Once these corrections have been made then RENUM renumbers and corrects the listings of the nodes and elements so that the output can go to the next program, LINEL.

### 3.4. LINEL

The LINEL program (Wilson, 1970) uses the output from RENUM for its input. The LINEL program first sorts the list of elements. The node numbers of the two nodes an element connects are arranged in an increasing order. The list of elements is arranged so the node number of the first of the two nodes it connects is in increasing order. For example, if element five connects nodes 6 and 5 and element six connects nodes 7 and 4, then the revised element list would have element five connecting nodes 4 and 7 and element six connecting nodes 5 and 6. The revised list is then used to fill the matrix and vectors that make up the system of linear equations to be solved for each node. The equations are based on the cubic law (Equation 2.1) with the unknown being the head or the flux depending on the boundary conditions. A mass balance is assumed at each node, the flow into each node equals the flow out of each node. The head at each node is

calculated and the flux through each element is found. The flux passing through a boundary is found by summing up the fluxes of the elements crossing the boundary. The head at specified boundaries as well as the flux crossing the boundaries forms the output from LINEL. The values of head and flux are solved at steady state flow conditions. The permeability is calculated four times, based on flow through the four sides of the flow region. The square flow region is rotated through a number of angles from 0 to 90 degrees and the permeability is measured at each fifteen degrees of rotation. In order for the flow region to be rotated and not extend beyond the generation region it must be smaller than the generation region by a factor of $\sqrt{2}$. These permeability measurements are used by the ELLFMG program.

### 3.5. ELLFMG

The permeability calculations in LINEL are made using Darcy's law, which is shown in Equation 3.1.

$$\frac{Q}{A} = K \frac{dh}{dl} \tag{3.1}$$

where:

$Q$ = Volumetric flowrate ($m^3/s$)

$A$ = Area of flow ($m^{2)}$

$K$ = Hydraulic conductivity ($m/s$)

$h$ = Hydraulic head ($m$)

$l$ = Flow path length ($m$)

For flow in the x direction Equation 3.1 can be written as

$$\frac{Q_x}{A} = K_{xx} \frac{\partial h}{\partial x} + K_{yy} \frac{\partial h}{\partial y} \tag{3.2}$$

where $Q_x$ is the flowrate in the x direction and $K_{xx}$ is the hydraulic conductivity in the x direction, which is also the hydraulic conductivity in the direction of the applied gradient, $K_g$. For the boundary conditions stated in Section 4.2.1. the term $\frac{\partial h}{\partial y}$ is zero. This simplified form of Equation 3.2 is used by LINEL to solve for $K_g$ through the four sides of the flow region at each rotation, from 0 to 90 degrees. A plot of $1/\sqrt{K_g}$ versus the angle of rotation on polar coordinates will result in a permeability ellipse (Marcus and Evanson 1961, Marcus 1962, Bear 1972).

The ELLFMG program (Long et al. 1982) creates the best fit permeability ellipse using directional permeability measurements of the flow region made in LINEL. The principal permeabilities, the maximum and minimum permeabilities, are calculated once all the permeability measurements have been made. The magnitude and direction of all the permeability measurements are the output of the ELLFMG program.

### 3.6. DIMES and ELLP

The DIMES and ELLP programs (Billaux et al. 1988) generate a graphic representation of the fracture mesh and the permeability ellipse, respectively. The input to DIMES is created by RENUM. The input to ELLP is created by ELLFMG.

### 3.7. TRINET

The TRINET program (Karasaki 1987) uses the finite element method (FEM) to solve transient flow calculations. The TRINET program was used to solve the head distribution as a function of time within the flow region. It is assumed that the flow through the fracture is laminar and that it follows the cubic

law. The permeability of the fracture system is assumed to be constant and not a function of pressure. This assumption would no longer be valid if the pressure within the fracture exceeded the overburden pressure. TRINET uses the Galerkin approach to solve the head at each node simultaneously. The output of TRINET is the head at each time step for any number of specified nodes.

### 3.8. PT

The PT program (Bodvarsson 1982) uses the integrated finite difference method (IFDM) to simultaneously solve mass and heat flow equations. The governing equations are for single-phase flow in a fully saturated media. At each time step the nonlinear equations are solved using an iterative scheme and an efficient sparse solver (Bodvarsson and Tsang 1982). The PT program was used to solve one dimensional transient mass flow in the meshes generated by the FMMG program.

### 3.9. FMMG

The fracture-matrix mesh generator, FMMG, (Karasaki 1987) is used to create a mesh that has a matrix, between fractures, permeable to flow and is used immediately following the execution of FMG. The FMMG program uses as its input the fracture geometry of the flow region calculated by FMG.

The first task of FMMG is to divide the matrix region between the fractures into convex polygons. To achieve this goal all the fracture dead ends are extended until they encounter a boundary or another fracture, either real or extended. These fracture extensions, can be considered imaginary fractures of zero aperture and they do not influence later flow calculations. The process of extending fractures is carried out until the flow region no longer has any fracture dead ends. The extension of a fracture will create a new element and probably a

new node. These are then added to the element and node lists.

The next step is to find the elements and nodes that form each polygon. This is done by starting at an arbitrary node and following the elements in a clockwise direction until reaching the initial node. This procedure is carried out until each element has been traced at least once in each direction. Once a polygon has been traced, the coordinates of the center of gravity and its area are calculated. The area distribution of the polygons are calculated once all the polygons have been traced and counted.

The area of the polygon near the fractures will be subject to large gradients. For this reason the polygons must be divided into smaller block elements. These block elements are made by drawing lines parallel to the elements that form the polygon. The spacing between these lines is an input parameter and it is suggested that a logrithmic spacing be used since the gradient will decrease rapidly as the distance from the fracture is increased. The sides of the block elements are created by rays extending from the center of gravity to the nodal points of the polygon. An example fracture-matrix mesh is shown in Figure 3.1.

The output from the FMMG program can be written for programs using the integrated finite difference method (IFDM) or the finite element method (FEM). The input for finite difference includes a listing of the nodal areas, block element connections, interface length and distance from the center of gravity to the block interface. The input for finite element includes a listing of the nodal coordinates and the element catalogue. The FMMG program also includes a graphics display of the generated fracture-matrix mesh.

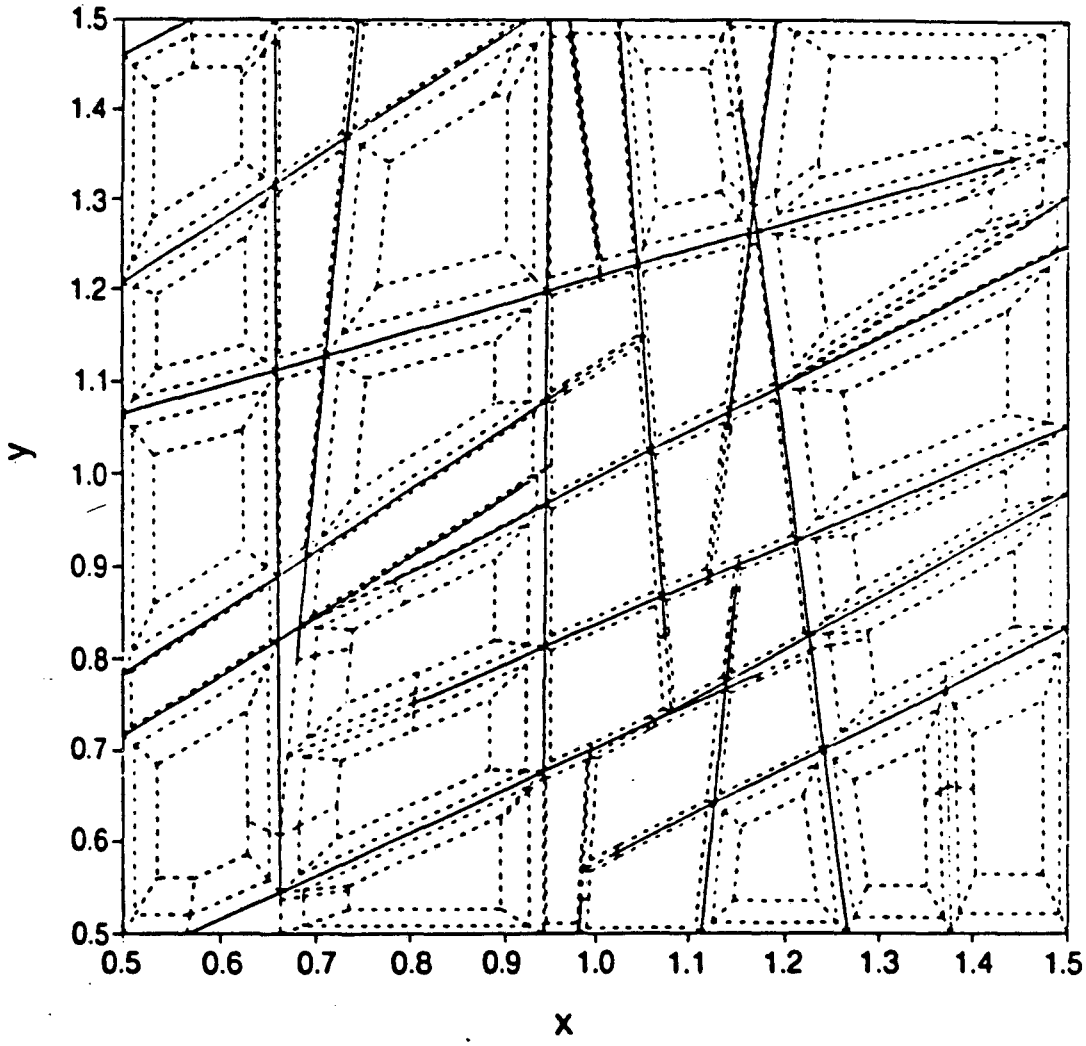


**Figure 3.1** Fracture-matrix mesh.

# CHAPTER 4

# HIERARCHICALLY FRACTURED SYSTEMS

## 4.1. Introduction

In nature, the sizes of fractures vary over orders of magnitude, from a small microfracture to a large fault. When trying to explicitly model flow through this rock numerically, it is impossible to model the whole range of fractures found in nature. It would therefore be beneficial to model only the range of fractures that most control flow.

In order to study which fractures most control flow, the following study was conducted. The purpose of this study was to determine the effect of fracture length and aperture on the permeability of a two dimensional fractured rock mesh. The possibility of replacing the short fractures with an equivalent porous medium was studied for both steady-state and transient flow conditions. Before presenting the study, it must be shown that the fracture-matrix meshes, which are used when the short fractures are replaced by an equivalent porous media, will give valid results when used with the PT program.

## 4.2. FMMG Mesh Validation

As explained previously, the PT program uses the integrated finite difference method (IFDM) to calculate the flow through a fracture-matrix mesh (Okusu et al. 1989). The meshes generated by FMMG do not meet the IFDM criteria that the connection between the nodes be perpendicular to the area of contact between these nodes. The amount of error introduced by not meeting this requirement will be examined. The FMMG program also discretizes the matrix blocks within a mesh into smaller blocks. It is a concern that the discretization step may

be another source of error that should be evaluated.

In order to estimate these two sources of error three different meshes were created. The aperture of the fractures within all of these meshes was constant and given a value of 50 micrometers. Using the cubic law shown in Equation 2.1, the permeability of a fracture with this aperture can be calculated to be 2.083E-10 $m^2$. The first mesh was created to act as a control mesh whose results would be compared with those achieved from the other two meshes. The control mesh was generated within the PT program and constisted of orthogonal fractures and square matrix blocks, resulting in a mesh consistent with the IFDM criteria. The control mesh is shown in Figure 4.1a. Both the fracture and matrix nodes were assigned a permeability of 2.083E-10 $m^2$.

The second mesh was created by the FMG and FMMG programs and is shown in Figure 4.1b. The FMG program placed fractures at random using a uniform distribution of orientation and length. The matrix between the fractures was separated into nodes and assigned a permeability of 2.083E-10 $m^2$ within the FMMG program. For this mesh the matrix was not discretized.

The third mesh consisted of the same fracture geometry as the control mesh. However, the matrix for this mesh was discretized by the FMMG program. The permeability of the matrix was also assigned to be 2.083E-10 $m^2$. The third mesh is shown in Figure 4.1c.

Although the fracture and matrix permeabilities of these three meshes are the same, the geometry of the fracture and matrix nodes is not. Each mesh was subjected to an identical flow test. A unit pressure gradient was imposed across the length of the meshes and the PT program evaluated the pressure increase at the downstream side of the mesh until the system reached steady state conditions. The pressure response curves for all three meshes are found in Figure 4.2. The non-orthogonal fractures of the second mesh produced a more jagged

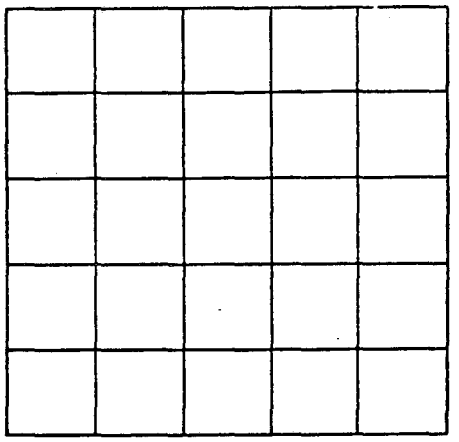

(a)

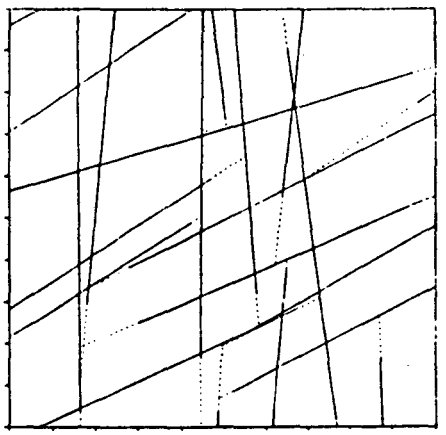

(b)

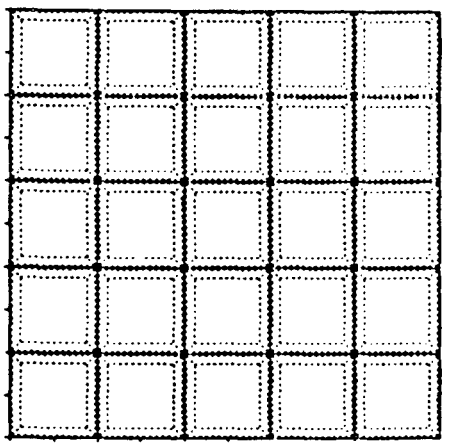

(c)

**Figure 4.1** (a) Control mesh. (b) Second mesh, with random fractures. (c) Third mesh, with discretized matrix.

pressure response curve. The shape of this curve could be due to the more complex geometry of this mesh which has nodes of various size and shape. The control mesh only has fracture nodes of one given length and matrix nodes of one given size.

The pressure response curve for the discretized mesh was the same shape as the pressure response curve of the control mesh but was always at a slightly lower pressure than the control mesh for any given time. The difference was probably due to numerical diffusion caused by a fewer number of nodes in the control mesh.

The deviations of the pressure response curves of the two test meshes from the control mesh curve were slight. It seems valid to use both non-orthogonal and discretized meshes in the PT program since the errors associated with them are small.

The PT program was used on meshes where the small fractures were replaced by an equivalent porous media. The first goal of the numerical study was to find the fracture length cutoff, below which the fractures could be replaced by an equivalent porous media and above which the fractures would have to be modeled explicitly.

## 4.3. Numerical Study

### 4.3.1. Mesh Geometry

The initial meshes used in the study were created by the FMG program using the following input parameters.

For all the meshes the generation region was set to 150 meters by 150 meters and the mesh region was defined to be 25 meters by 25 meters. The total number of fractures within the generation region was about 42,000 and resulted in

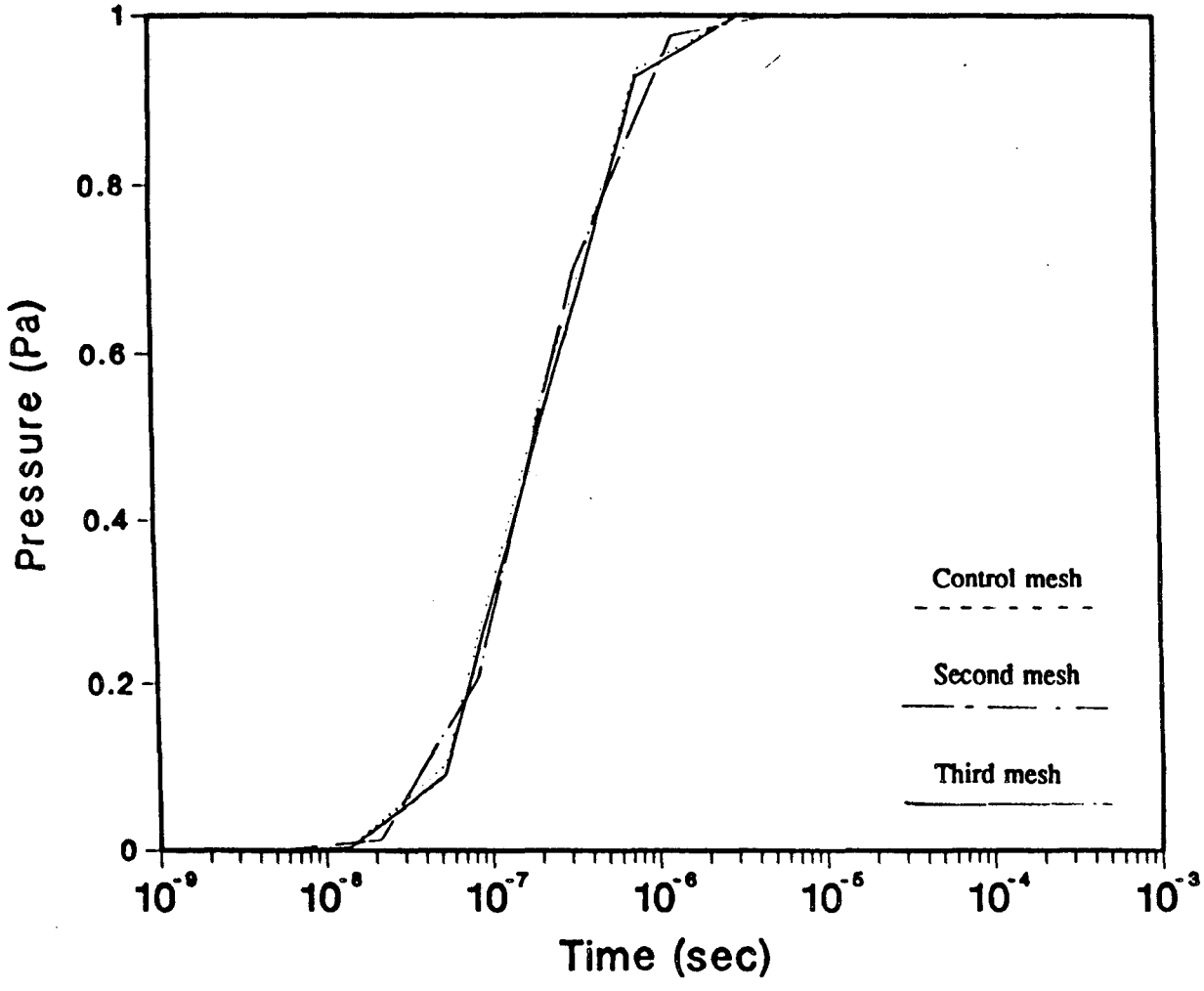


**Figure 4.2** Pressure response curves of three different mesh geometries.

a well connected mesh. The mesh region contained over one thousand fractures.

The boundary conditions for all the flow tests carried out on the meshes was the same. The left and right boundaries of the mesh region were assigned constant head values of one meter and zero meters of water, respectively. The upper and lower boundaries had a linearly distributed head from one meter to zero meters of water, going from left to right.

The fracture orientation distribution for all the meshes was the same. The orientations of all fractures were uniformly distributed from zero to one hundred eighty degrees.

The same fracture length distribution was used in all of the meshes. The fracture length distribution, $f(l)$, was chosen as follows. First a negative exponential distribution, $f(l) = e^{-0.5l}$, was chosen. This distribution gives a large number of short fractures and a small number of long fractures. Then the fracture length distribution was divided into sets. The range of these sets and the fracture density for each set, calculated from the negative exponential distribution, are shown in Table 4.1. Within each set the fracture length is uniformly distributed over the range of that set. As seen in Figure 4.3 the joining of these uniform distributions approximates a negative exponential distribution.

The fracture aperture directly affects the overall permeability of a mesh, so three different methods were used to choose the fracture aperture. The first method assigned a constant aperture of 50 micrometers to all fractures. The second method used the same negative exponential distribution of aperture for each fracture length set: $f(b) = e^{-2E+04b}$. The third method used the same distribution as the second method but in this case the aperture was correlated to the fracture length, such that short fractures had small apertures and long fractures had large apertures. In all cases the mean of $b^3$ was held the same so the overall permeabilities were the same. These three aperture types will be referred to as

**Table 4.1** Fracture length and density distribution

| Range of Fracture Length (m) | Fracture Density |
|---|---|
| 0.0 - 0.1 | 4.9% |
| 0.1 - 0.2 | 4.6% |
| 0.2 - 0.4 | 8.6% |
| 0.4 - 0.8 | 14.8% |
| 0.8 - 1.6 | 22.1% |
| 1.6 - 3.2 | 24.7% |
| 3.2 - 6.4 | 16.1% |
| 6.4 - 12.8 | 3.9% |

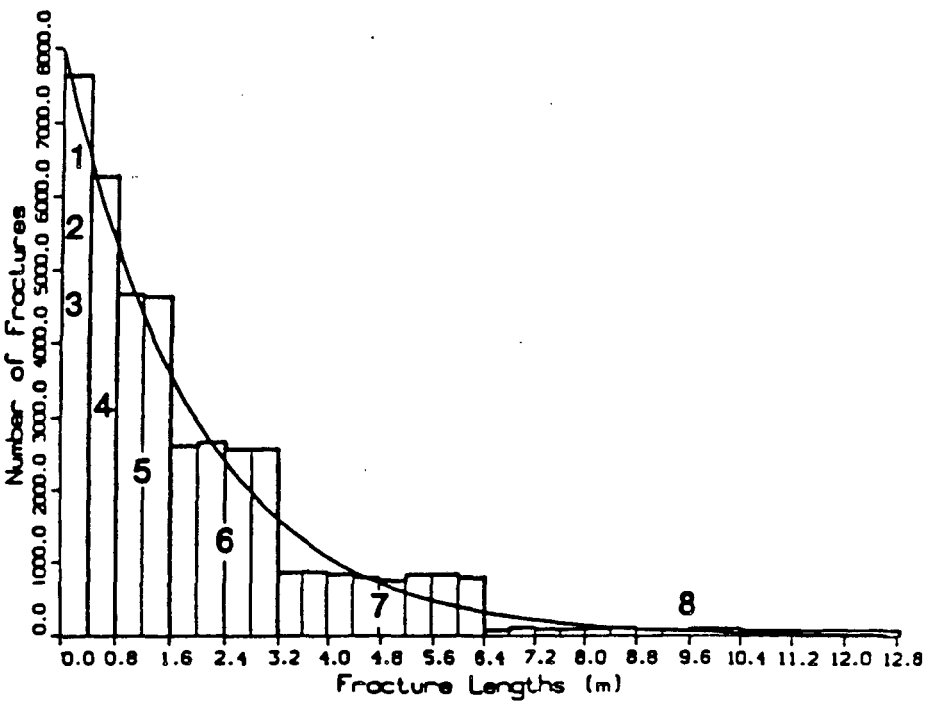


**Figure 4.3** Negative exponential distribution and the generated fracture sets.

constant aperture, distributed aperture and correlated aperture, respectively. For each aperture method at least three different meshes were generated.

### 4.3.2. Procedure

For each aperture distribution the following tests were carried out on at least three different meshes. First, a fracture mesh was generated by the FMG program to create an initial mesh with all eight fracture length sets. Then the RENUM program was run to renumber the nodes and to remove any inherent problems within the flow region. A flow calculation was run on the flow region by the LINEL program, which solves for the steady state flow rate within the flow region. The ELLFMG program calculated the permeability of the mesh. The geometrical mean permeability, ie. the square root of the product of the principal permeabilities, was calculated and used to represent the overall permeability of the mesh. Both the DIMES and ELLP programs were executed to get graphical representations of the mesh and permeability ellipse, respectively.

This series of programs were then executed again on the same mesh, ie. the same random seed, with the exception that the smallest fracture length set was removed. Next the smallest two sets were removed etc. The process of removing a fracture length set and recalculating the mesh permeability was continued until the mesh contained only one set of fractures, the longest fractures. This gives permeability as a function of $l_t$, the truncation length, where fractures shorter than $l_t$ have been eliminated. An example of the eight meshes created by this procedure is pictured in Figure 4.4.

### 4.3.3. Results

Plots of the overall mesh permeability versus $l_t$ were constructed. Three runs for each aperture distribution are shown in Figure 4.5.

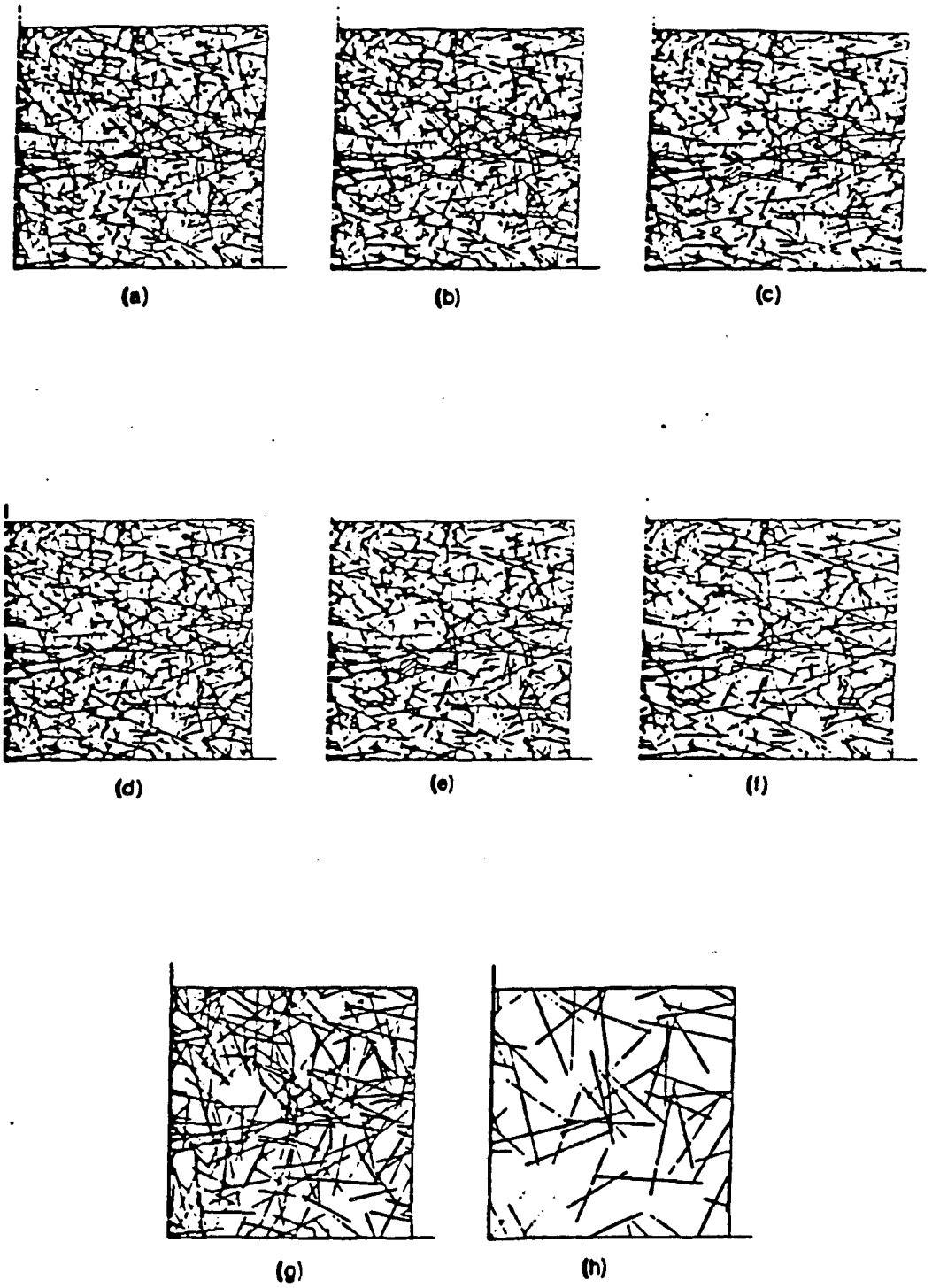


**Figure 4.4** Fracture meshes with decreasing number of sets from (a) to (h).

For constant aperture the permeability of each run was approximately the same regardless of the number of meshes generated. The permeabilities for the other two aperture distributions had a higher variance. The permeabilities of the correlated meshes tended to be about an order of magnitude greater than the permeabilities of the constant or distributed apertures. The increase in permeability for the correlated aperture is due to the chance of large fractures having large apertures connecting to form paths of large permeability.

The shape of all the fracture length versus permeability curves are similar, regardless of the aperture distribution used. The curves are flat with a sudden drop at larger fractures lengths, 3.2 meters to 12.8 meters. These drops in the permeability curves, once fractures beyond a certain cutoff length are removed, are observed by Hestir and Long (1990). The flatness of the curve up to 3.2 meters indicates that the permeability stays essentially constant while 80% of the fractures are removed. The drop in the curve is a measure of the degree to which the permeability is controlled by the largest fracture set. A small drop in permeability indicates a large dependence on the longer fractures. The correlated aperture distribution has the smallest drop in permeability which indicates that the largest fractures greatly affect the permeability of the meshes. This result is in agreement with the conclusion drawn from the observed higher permeabilities of the correlated aperture meshes mentioned previously.

### 4.4. Equivalent Porous Media

The results indicated that at least 80% of the fractures had no effect on the overall permeability of the meshes. The feasibility of replacing the short fractures by an equivalent porous media was studied for steady state and transient conditions.

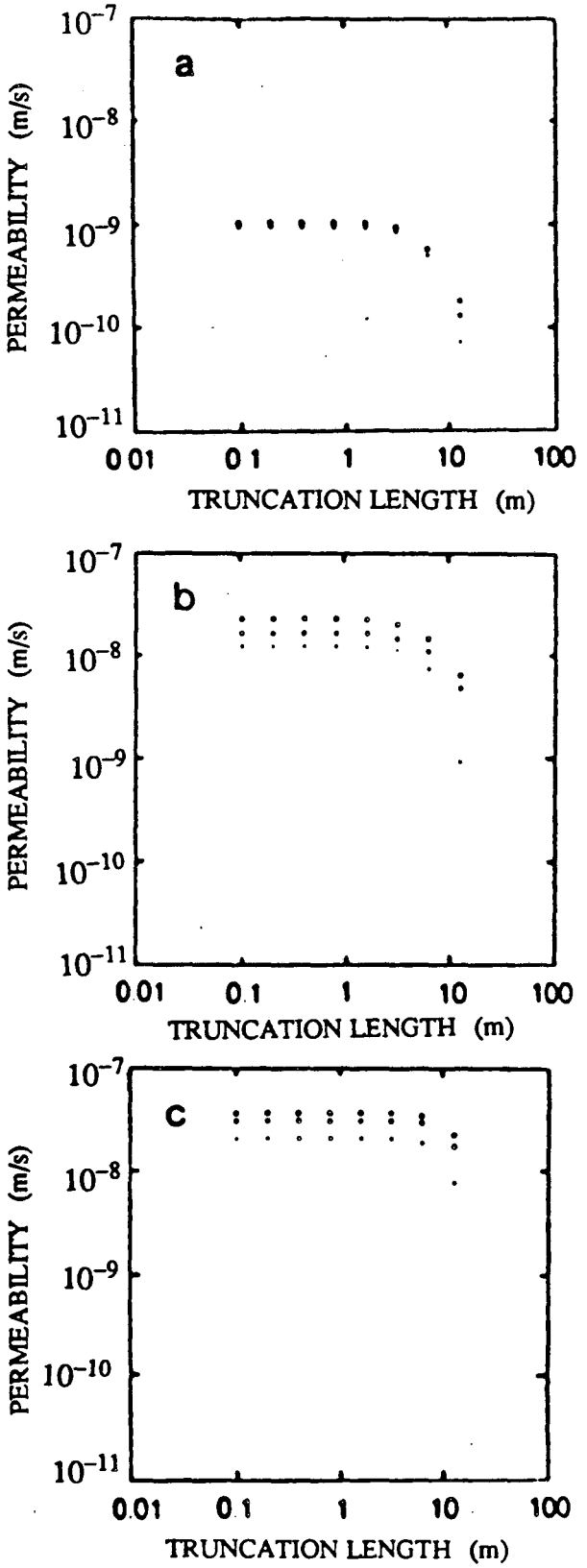


**Figure 4.5** Permeability vs. truncation length with (a) constant aperture, (b) distributed aperture, (c) correlated aperture.

### 4.4.1. Steady State Conditions

One of the constant aperture meshes was selected to have all but the longest length fractures (6.4 m to 12.8 m) replaced by an equivalent porous media. This porous media substitution was for 96% of the original fractures. The resulting mesh had only long fractures and the matrix between the fractures represented the porous media. The substitution caused a significant decrease in the number of nodes within the mesh. The fracture-porous media mesh was constructed by the FMMG program. It was desired to try to create a fracture-porous media mesh with the same overall mesh permeability as the fracture only mesh at one dimensional steady state flow conditions. To achieve this goal the porosity and permeability of the porous media blocks needed to be found. The porous media blocks' porosity was calculated by dividing the volume of the deleted fractures by the volume of the matrix blocks. The result is a constant average porosity for all the porous media blocks which is used as input for the PT program.

The permeabiltiy of the porous media blocks was found by a trial and error method. An arbitrary, constant value of permeability was chosen for the porous media blocks. A flow test was then run on the mesh, using the PT program, until the system reached a steady state condition. The steady state flow rate was known so the overall permeability of the mesh could be solved using Darcy's law, see Equation 3.1. The overall permeability was compared to the overall permeability of the fracture only mesh containing all the fracture sets. If the permeabilties were not in close agreement then the porous media permeability was changed and the procedure was repeated to find a new overall permeability of the fracture-porous media mesh. This was continued until the overall permeabilites of the two meshes were approximately equal. The final fracture-porous media mesh created not only gave a value for the permeability of the porous media blocks, equal to 6.122E-15 $m^2$, but also represents a mesh with the same apparent overall

hydraulic properties at steady state as the original fracture only mesh.

### 4.4.2. Transient Conditions

In order to study the mesh under one dimensional transient flow conditions, the TRINET program was run using the fracture only mesh containing all the fracture sets and the PT program was run using the fracture-porous media mesh. The boundary conditions of both meshes were the same. A constant head of one meter of water was set on the left side and a constant head of zero meters of water was set on the right side. The upper and lower boundaries were made impervious to flow. The two meshes are pictured in Figure 4.6, which also shows two nodes within each mesh specifically labelled. The nodes marked A and A' are on the same central fracture in both meshes, so the pressure behavior at that fracture can be compared between the two meshs. The nodes marked B and B' are in the same relative location in each mesh. Node B is located on a small fracture and node B' is on the porous media that replaced that and any neighboring small fractures. The pressure response curves at these nodes will be compared.

The pressure heads at these four nodes are plotted as a function of time and are shown in Figure 4.7. The head at node A' does not asymptote to the same steady state value as that of node A. The difference in these steady state values was due to the averaging of the permeability of all the small fractures into a porous media permeability for the fracture-porous media mesh. For the fracture only mesh the permeability is not as uniformly distributed, due to the presence of the small fractures, as it is for the fracture-porous media mesh. If the same flow test was executed on a non-fractured porous media mesh, which would have a constant uniform overall permeability, the pressure head would decrease linearly from one to zero for an incompressible fluid, going from left to right. Once fractures are introduced, the permeability fails to be constant throughout the mesh and

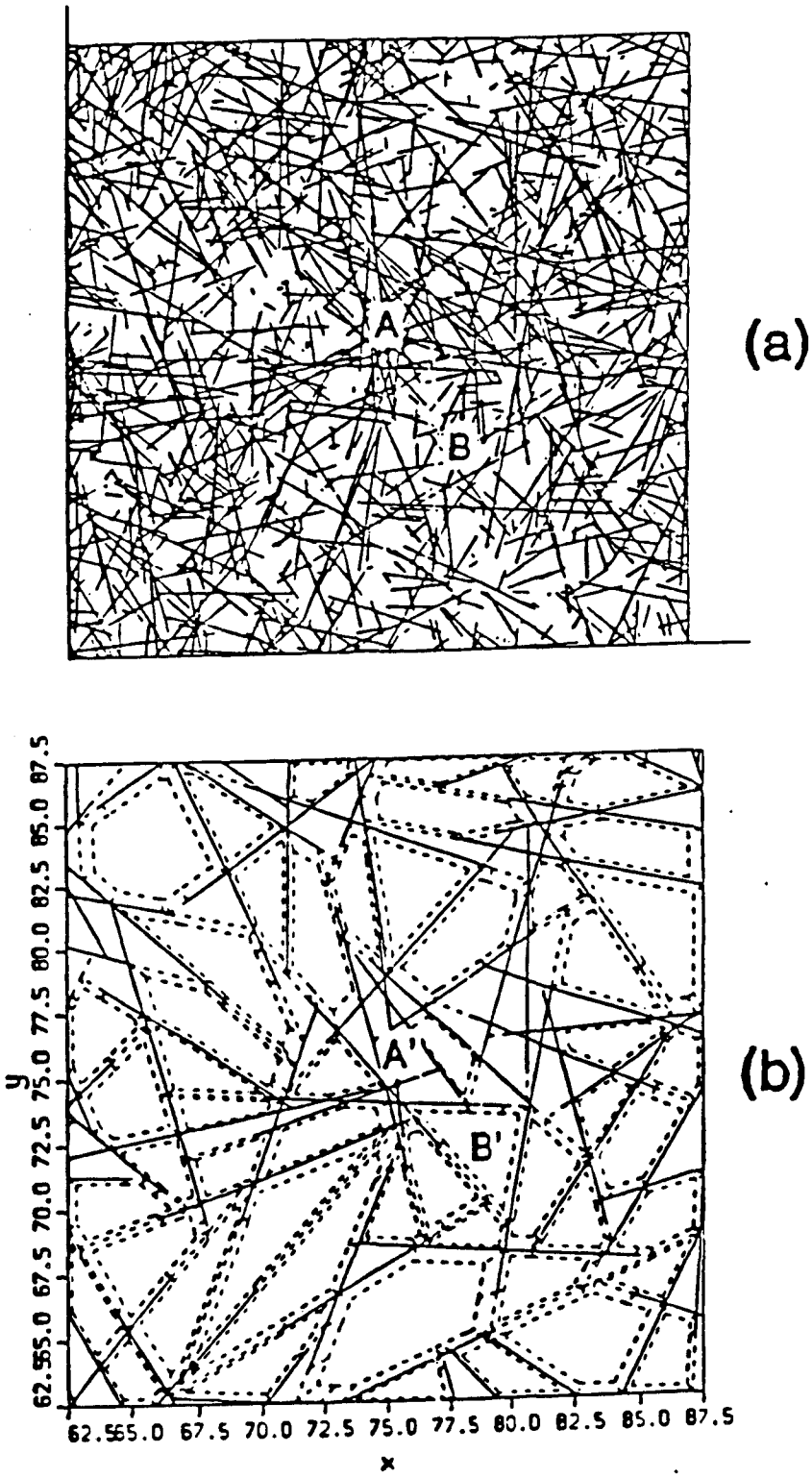


**Figure 4.6** (a) Mesh with all the fractures. (b) Mesh with small fractures replaced by blocks of porous media.

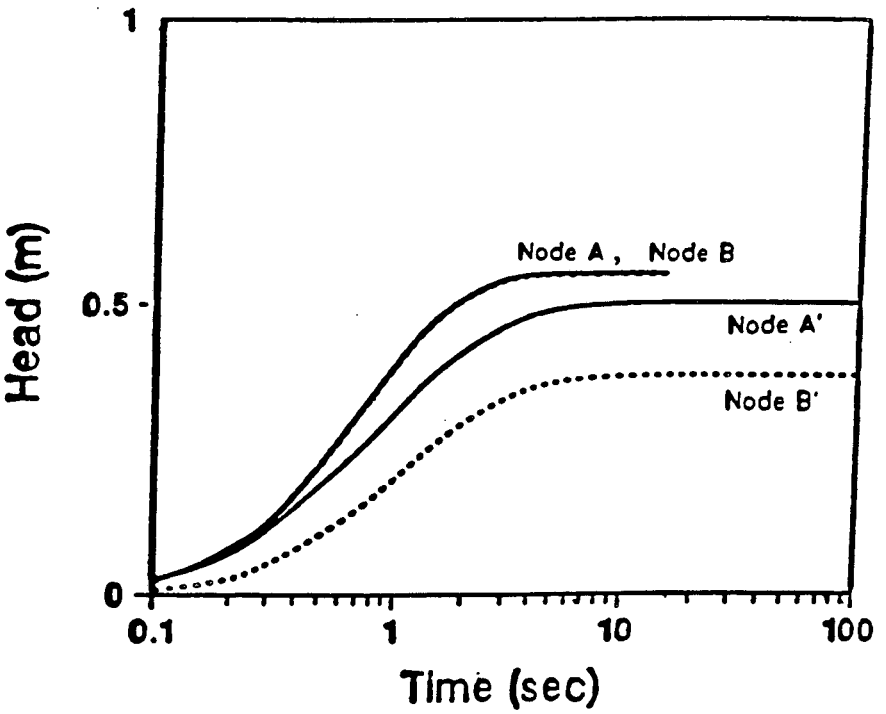


**Figure 4.7** Transient pressure response curves at Node A and B in the fracture only mesh and Node A' and B' in the fracture porous media mesh.

the pressure head between the boundaries will no longer decrease linearly. The fracture-porous media mesh behaves more like a continuous porous media than the fracture only mesh, so its central node A' asymptotes to a value of 0.5 meters of water. The fracture only mesh asymptotes to a larger value of about 0.6 meters of water. The higher pressure head at node A was due to the left half of the fracture only mesh being more permeable than the right half.

The head at node B' of the fracture-porous media mesh built up slower and asymptotes to a lower value than node A' because node B' was hydraulically downstream with respect to node A'. The head at node B of the fracture only mesh follows the same behavior as node A. Although node B is geometrically downstream of node A, it is not hydraulically downstream due to the small fractures causing local discontinuities and preferred flow paths.

### 4.5. Conclusions

In this study it was found that short fractures may be relatively unimportant for steady state flow calculations. By replacing these short fractures by an equivalent porous media the number of nodes within the mesh was significantly reduced, which decreased the time and memory storage needed to numerically model the systems. For the twenty-five meter square mesh region modeled in this study it was found that fractures on the order of one fourth of the mesh length or longer were the only fractures that needed to be explicitly modeled. The remaining fractures could be modeled by equivalent porous media. If this conclusion holds some generality, it would be useful for field geologists mapping fractured outcrops for later computer simulation. The geologist would only have to map fractures whose lengths were about one fourth of the mapping regions length or longer. This could decrease the time spent mapping each region as well as the time spent later modeling these regions.

The replacement of small fractures by equivalent porous media blocks may not be valid for transient flow conditions. It was found that the local heterogeneities of a fracture only mesh were not reproduced in the fracture-porous media mesh. The averaging of the small fractures into porous media blocks resulted in nonequivalent meshes when individual nodes were studied. The meshes may be less equivalent for mass transport problems. For mass transport problems the paths available for transport will dictate the results. In a fracture-porous media mesh the paths available for flow are fewer and less complicated than a fracture only mesh. The variations in results of mass transport tests on these meshes could be quite high.

The validity of using porous media blocks in place of short fractures seems to be scale dependent. If the overall mesh properties are the only concern then the substitution seems valid. If details within the mesh are to be studied then the substitution may not be valid.

These conclusions are only pertinent for this study and cannot be generalized until more work has been done to make a quantitative assessment. Future studies should include some work with mass and heat transfer processes.

# CHAPTER 5

# FRACTAL ROCK SYSTEMS

## 5.1. Introduction

Fluid flow through rock systems has, traditionally, been modeled in systems with a Euclidean dimension. That is, one with an integral dimension of either one, two or three. In the previous chapter's study the fracture length distribution was selected to give fracture meshes that were well connected, resulting in fracture meshes with an Euclidean dimension of two. The emphasis in this study will be the flow characteristics of rock systems with fractures that are not well connected. These can be considered as non-Euclidean, or fractal systems. Two types of rock systems, both having fractal properties, will be used in this study.

The purpose of the study was to calculate flow dimensions for computer generated fractal rock systems, having known fractal dimensions, and then compare these flow and fractal dimensions. The flow dimension will be defined later and described in greater detail. The study will be presented as described below, starting with a brief introduction to, and the motivation behind, the work that was done in this study, followed by a description of the well tests that were modeled on rock systems having fractal structures. The theories behind the two types of fractal rock systems will be explained before describing the actual rock systems and the methods of generating these systems. The method used to calculate the fractal dimensions of these systems will then be explained. The background and method of calculating the flow dimension will then be presented. A generalized solution of flow during a well test is used to find the flow dimension. This solution will be shown and the flow dimension will be defined. The results of the study will be presented as a comparison between the fractal dimensions and the

flow dimension of various rock systems.

## 5.2. Background

Before discussing the details of the study, it is important to stress that numerical analysis of fluid flow in fractured rock presents difficulties which stem from the fact that the geometry of fractured rock is generally unknown and complex. Some of the complexity of fracture geometry is due to the fact that fractures exist at all scales. There are faults on the order of hundreds of kilometers in length on one end of the spectrum, and there are small microfractures at the rock grain on the other end. Since the fracture geometry is complex and fractures are at all scales, one promising approach is to treat fracture systems as fractals. It has been observed in natural rock that the trace length distributions do, in fact, exhibit fractal characteristics (Barton 1987). Therefore, it seems reasonable to use fractal rock systems to model natural rock. These fractal rock systems were created by a computer and used to model well tests numerically.

The purpose of the well test is to gain an understanding of flow behavior through the rock. A constant flow rate injection well test was modelled in this study. This type of well test consisted of injecting fluid into the system by pumping fluid into the well at a constant flow rate. Information about the overall flow properties of the rock surrounding the well can then be gained by monitoring the resulting change in pressure.

Once the initial rock systems were created they were given as input to the RENUM program, which eliminated dead-end fractures and efficiently renumbered the nodes and elements. The TRINET program was then used to numerically model the well test. The input flowrate at the well was $5.0E{-}05m^3/s$. The pressure head as a function of time was calculated at every node. The pressure response at the well was plotted on log-log paper as a function of time.

### 5.2.1. Percolation Theory

Imagine a grid of squares drawn on a piece of paper (Figure 5.1a). If some of the sides of the squares within the lattice were erased at random, then something resembling Figure 5.1b would result. The remaining sides of the squares form what are known as clusters. A cluster can range in size from an isolated side of a square to an infinite number of square sides connected to each other. Percolation theory deals with describing the number and behavior of these clusters.

The lattice described is an example of bond percolation, which was the type used in this study. There are some differences between bond percolation and its counterpart, site percolation, but only bond percolation will be discussed from now on. The sides of the squares in the lattice are called bonds. The bonds that remained are open bonds and the ones erased are closed bonds. Each bond has a probability, $p$, of being an open bond and a probability, $1 - p$, of being a closed bond. Given an infinite lattice there is a unique probability at which an infinite cluster will appear. An infinite cluster is a cluster that spans an infinite lattice. The probability at which this will occur is called the critical probability and is denoted $p_c$. For an infinite lattice, if the probability is above the critical probability, $p > p_c$, an infinite cluster will appear with probability one. If the probability is below the critical probability, $p < p_c$, then an infinite cluster will appear with probability less than one. When numerically modeling, however, one works with finite lattices. A finite lattice can be thought of as a window looking upon part of the infinite lattice. If the window falls on the infinite cluster then a cluster will appear that spans the finite lattice. It is also possible for the window to fall on a finite cluster that may not be big enough to span the finite lattice. In other words, when working with finite lattices the critical probability will not result in a distinct cutoff between percolating and nonpercolating networks.

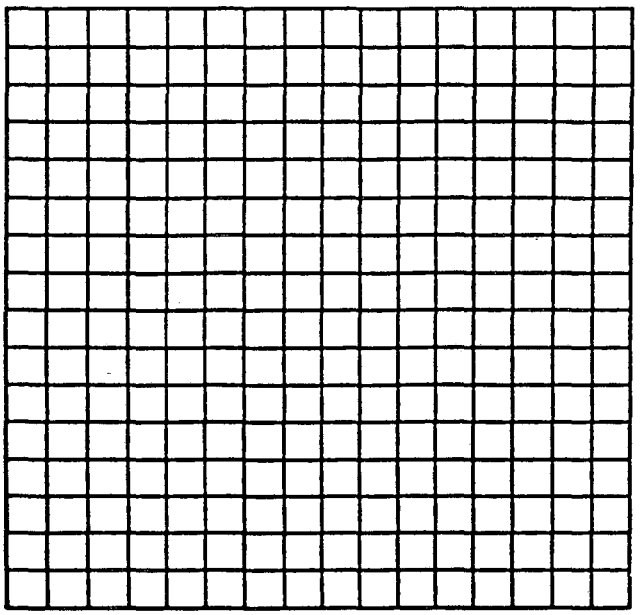

(a)

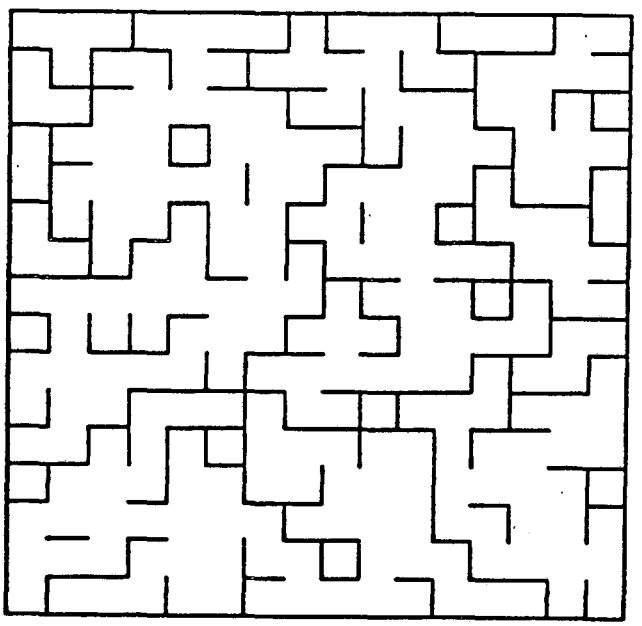

(b)

**Figure 5.1** (a) Square lattice. (b) Percolation clusters.

The importance of percolating networks is that they have a "self-similar" geometry within a range of lengths, $l$. A self-similar geometry means that the structure's geometry appears the same at any length scale, within the specified range, and exhibits fractal characteristics. The lower limit of the self-similar range is the bond length, denoted as $a$. The upper length limit is called the percolation correlation length, $\xi_p$, and is found from Equation 5.1.

$$\xi_p \sim a \, | p - p_c | ^{-\nu_p} \tag{5.1}$$

The value of $\nu_p$ is believed to be exact and equal to $\frac{4}{3}$. For the square lattice described earlier the critical probability equals 0.5 and the bond length can be taken to be unity. If a percolating network were constructed with $p = 0.65$ then, from Equation 5.1, the network would be fractal within the range $1 \leq l \leq 12.55$. The length $l$ can be thought of as the length of a side of a percolating network. The portion of the network within the range $a \leq l \leq \xi_p$ will be fractal and the portion of the network within the range $l \geq \xi_p$ will be homogeneous.

### 5.2.2. Sierpinski Carpet

The second rock system was generated by modifying the well known Sierpinski carpet. The theory and construction of a Sierpinski carpet has been described by many, Mandelbrot (1982) and Feder (1988). An outline of the theory used to construct a Sierpinski carpet and an example of such a carpet are given below.

Consider a finite piece of a line. The points defining the line piece are contained in a set $S$. Now if the line piece were scaled down by a factor, $r$, which is less than one, then the points contained by this new line segment make up the set $S' = rS$. The set $S'$ will always be a subset of $S$ and the line segment

described by $S'$ will only cover part of the original line piece. Now if r was cleverly chosen then the original line piece could be covered once by a series of nonoverlapping line segments. The number of line segments needed to cover the line piece will be denoted by $N$. If a line piece of unit length is considered then $\frac{1}{N}$ is one appropriate expression for the scaling ratio, $r$. For a unit rectangular piece of a plane to be covered by scaled down rectangles an $r(N) = \left[\frac{1}{N}\right]^{\frac{1}{2}}$ is an appropriate scaling ratio. Similarly, a unit rectangular parallelpiped can be covered if $r(N) = \left[\frac{1}{N}\right]^{\frac{1}{3}}$ is chosen. These three scaling ratios can be described by

$$r(N) = \left[\frac{1}{N}\right]^{\frac{1}{d}} \tag{5.2}$$

where $d$ is equal to the Euclidean dimension of one, two or three for lines, planes and cubes, respectively. This relation can be generalized to

$$r(N) = \left[\frac{1}{N}\right]^{\frac{1}{D}} \tag{5.3}$$

where $D$ is a positive real number. If $D$ is equal to an integer then $D$ will equal the Euclidean dimension. If $D$ is nonintegral then it is known as the fractal dimension.

To generate systems that have a fractal dimension first solve for $D$.

$$D = \frac{\ln\left[\frac{1}{N}\right]}{ln(r(N))} = \frac{\ln(-N)}{ln(r(N))} \tag{5.4}$$

Now choose an $r(N)$ and $N$ so that the ratio of their natural logs is not equal to an integer. To illustrate this point let us look at the construction of a Sierpinski

carpet.

The unit rectangular piece of a plane used to generate the carpet is called an initiator. The initiator in this case is a filled square and is pictured in Figure 5.2a. The set of nonoverlapping scaled down squares is known as the generator and is pictured to the right of the initiator in Figure 5.2b. The generator is made up of nine scaled down squares with the central square removed. The scaling ratio is $r = \left[\frac{1}{9}\right]^{\frac{1}{2}} = \frac{1}{3}$. The value of N is nine, if all the squares are filled, but the central square is not filled so $N = 8$. Figure 5.2 shows the carpet up to the fourth construction stage. The fractal dimension of a carpet at an infinite number of construction stages can be calculated from Equation 5.4.

$$D = \frac{ln(-8)}{\ln\left[\frac{1}{3}\right]} = \frac{ln\,8}{ln\,3} \sim 1.89$$

The details of the Sierpinski carpet used in this study will be explained in a later section.

### 5.3. Percolating Network

The well tests were performed on two different types of fractal rock systems based on the two theories of fractal structure just presented. The first of these fractal rock systems was based on percolation theory. The lattice used consisted of equilateral triangles. The sides of the triangles were considered to be bonds that had a probability $p$ of being open bonds and a probability $1 - p$ of being closed bonds. The open bonds were considered to be unit length fractures. The rock system was created by keeping these open bonds. The rock system was then further refined by keeping only the fractures on the backbone cluster. The backbone cluster consisted of all flow paths connecting the centrally located well

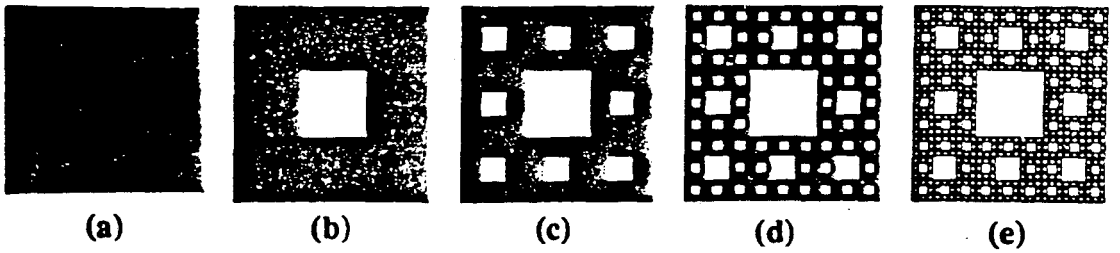


**Figure 5.2** Sierpinski carpet for $N = 8$ (a) carpet initiator, (b) carpet generator, and (c)-(e) carpet construction stages.

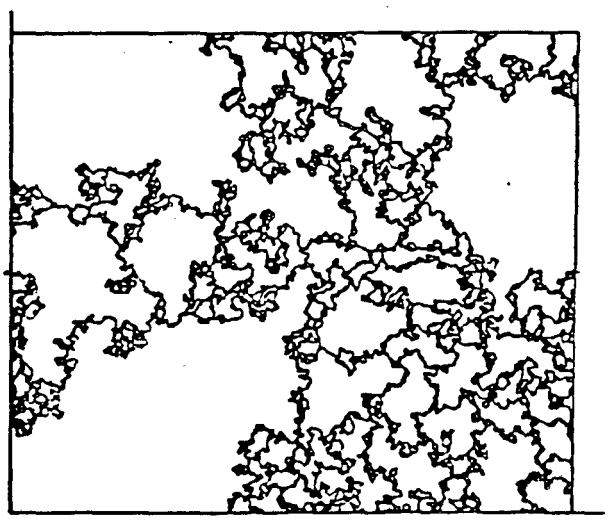

**Figure 5.3** Backbone cluster of percolating network.

to a boundary. Figure 5.3 shows an example network, which consists of just the backbone cluster. The network shown is 243 unit length fractures across.

The critical probability for an equilateral triangular lattice, using bond percolation, is 34.73%. The percolating networks were created with $p$ close to the critical probability so the networks would have self similar geometry and would exhibit fractal properties.

There were two different sized percolating networks used for this study. The networks shown in Figure 5.4 are 64 unit length fractures across and the ones shown in Figure 5.5 are 243 unit length fractures across.

### 5.4. Modified Sierpinski Carpet

The second fractal system was constructed by modifying a Sierpinski carpet. The carpet was modified by substituting lines, which represent fractures, for the filled in square regions. Each line is a set of fractures placed end to end without overlapping. There are four of these fracture sets placed in a square. They are evenly spaced with two sets horizontal and two sets vertical and resemble the set up of a tick-tack-toe game. The initiator of a modified Sierpinski carpet is shown in Figure 5.6a. The generator, for $N = 5$, is pictured in Figure 5.6b and is followed by meshes up to the fourth construction stage (Figures 5.4c - 5.4e). The scaling ratio for the mesh shown is $r = \left[\frac{1}{9}\right]^{\frac{1}{2}} = \frac{1}{3}$. The value of $N$ varies depending on how many squares are chosen to be fractured.

The modified Sierpinski carpet mesh pictured in Figure 5.6 is generated by always picking the same five locations to place fractures. It is not necessary to always pick the same locations as long as the number of squares to be fractured, $N$, stays the same for each construction stage. The modified Sierpinski carpet meshes used in this study were created by randomly picking $N$ locations at each

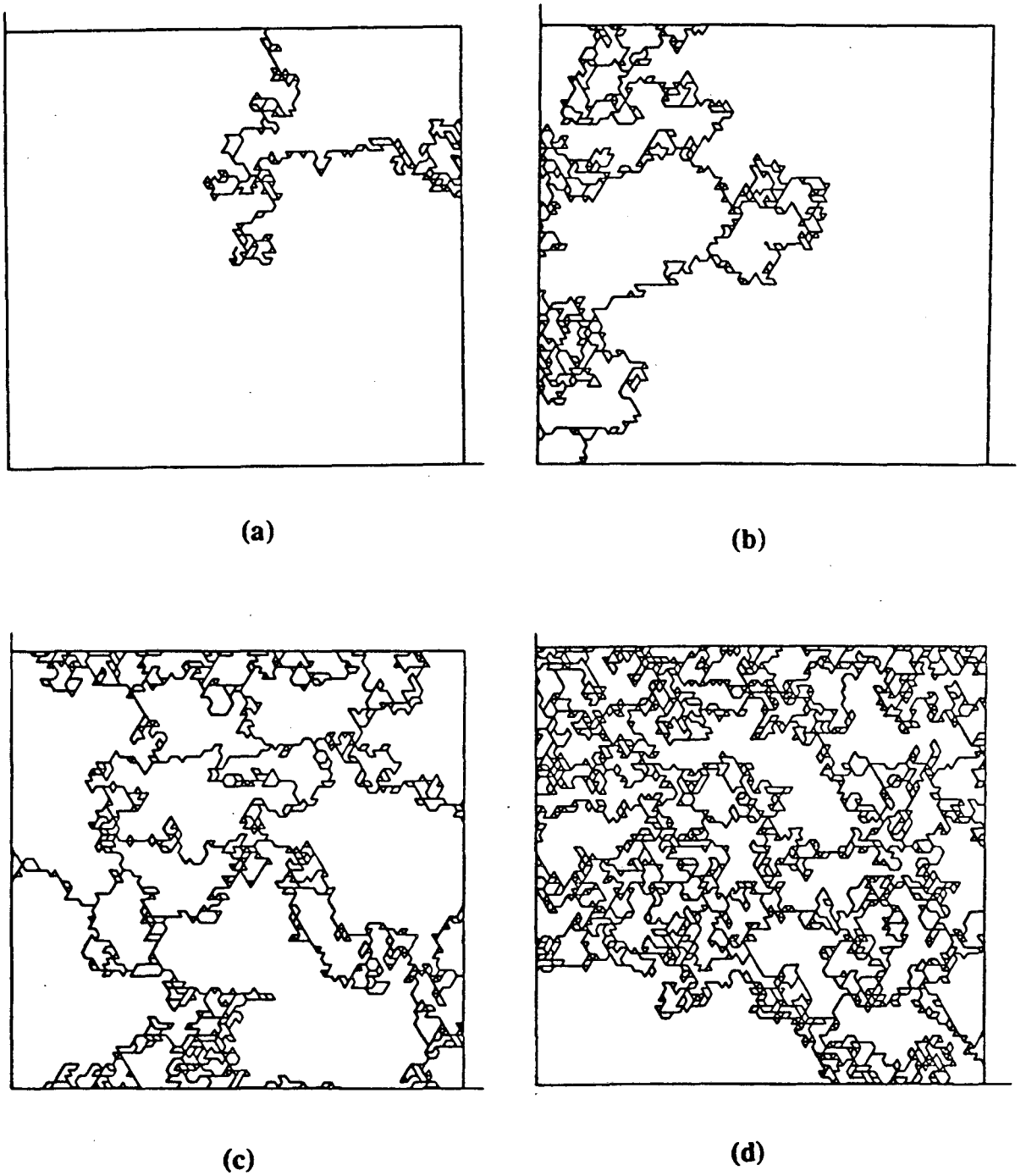


**Figure 5.4** Percolating networks that are 64 unit length fractures across (a) $p = 0.3473$, (b) $p = 0.3450$, (c) $p = 0.3500$, and (d) $p = 0.4000$.

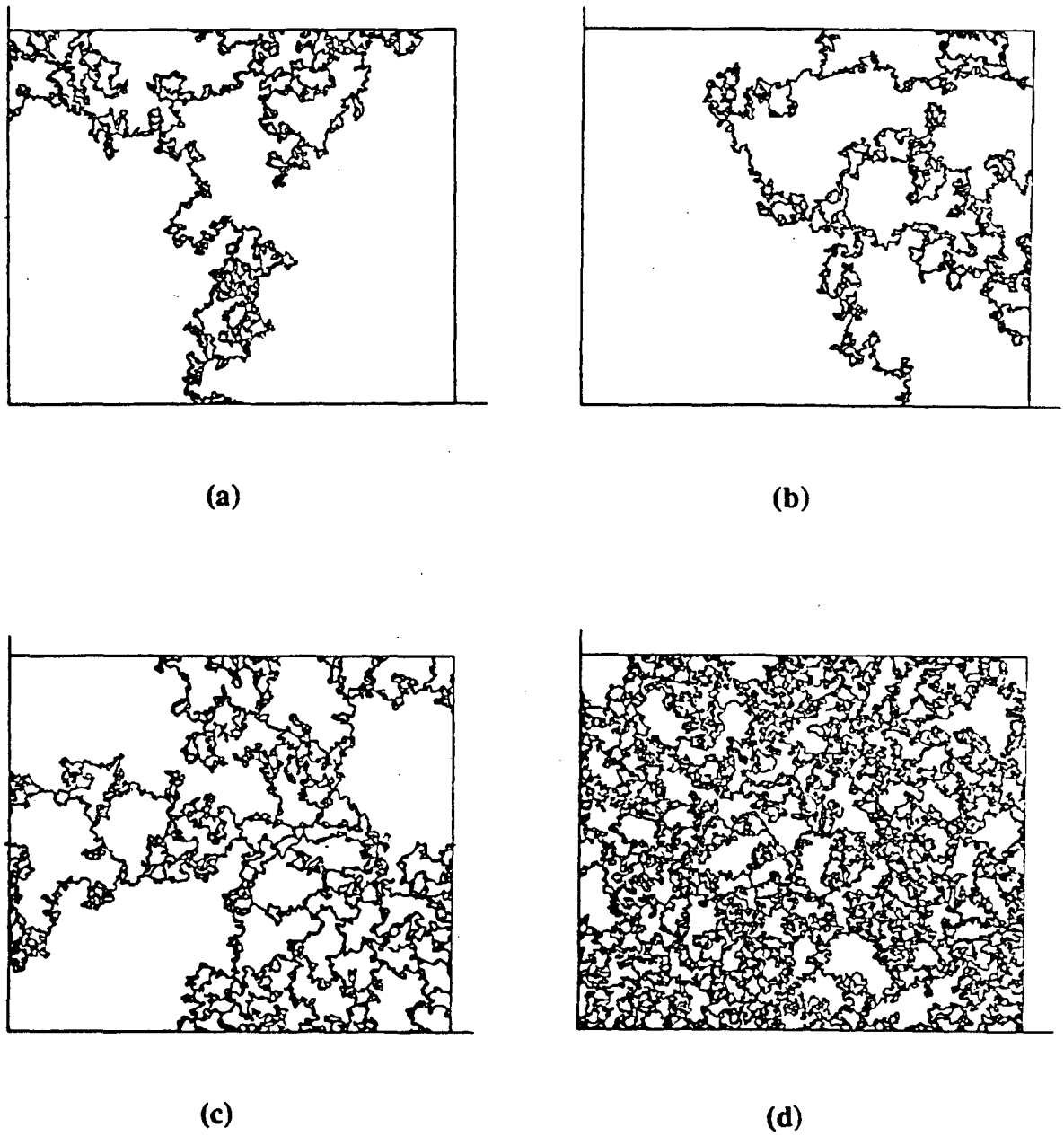


**Figure 5.5** Percolating networks that are 243 unit length fractures across (a) $p = 0.3473$, (b) $p = 0.3450$, (c) $p = 0.3500$, and (d) $p = 0.3800$.

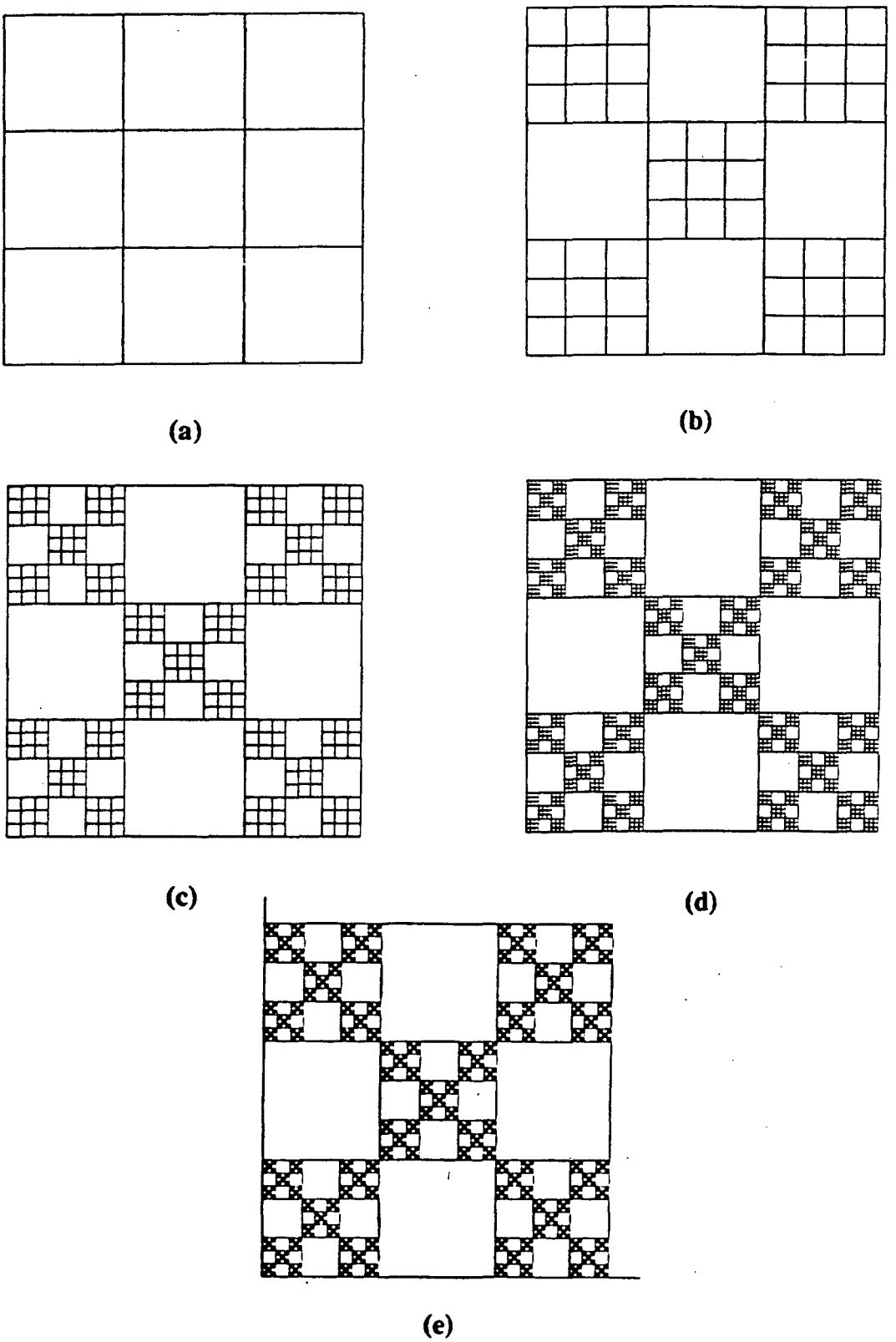


**Figure 5.6** Modified Sierpinski carpets for $N = 5$ (a) carpet initiator, (b) carpet generator, and (c)-(e) carpet construction stages.

construction stage. An example of these randomly fractured meshes is shown in Figure 5.7. The carpet has six of its squares fractured ($N = 6$) at each construction stage and is shown here at the fourth construction stage, which is the limit of the computer memory. At this stage the smallest fracture is designated to be one unit in length and the sides of the carpet consist of 243 unit length fractures. A central fracture was needed for the point of injection during a well test. To create a mesh having a central fracture, a number of meshes were created until a mesh was found with a fractured central square at each of the four construction stages. The search was continued until seven meshes with central fractures were found for each value of $N$. One of these seven meshes, at each value of $N$, is presented in Figure 5.8.

If the fracture mesh pictured in Figure 5.7 consisted of an infinite number of constuction stages then, according to Equation 5.4, it would have a fractal dimension of $D = \frac{ln\,6}{ln\,3} \sim 1.631$. However, all the meshes created were finite in extent so it is not valid to use Equation 5.4 to calculate the fractal dimension. The method used to calculte the fractal dimensions of the modified Sierpinski carpets and the percolating networks is explained in the following section.

### 5.5. Fractal Dimension

The fractal dimensions of the two rock systems just described can be found by calculating the fracture density as a function of distance from an assigned origin. The density of a fractal network will decrease as the length scale increases, unlike an Euclidean network which has a constant density with increasing length scale. The mass, $M$, of a fractal structure contained within a sphere of radius r is

$$M(r) = Lr^D \tag{5.5}$$

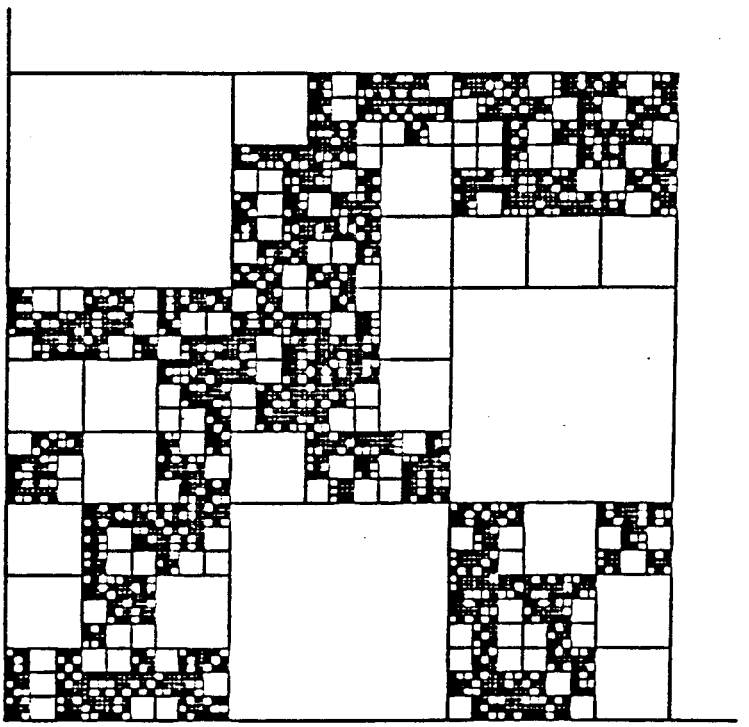

**Figure 5.7** Modified Sierpinski carpet for $N = 6$ and with the fractures placed at random.

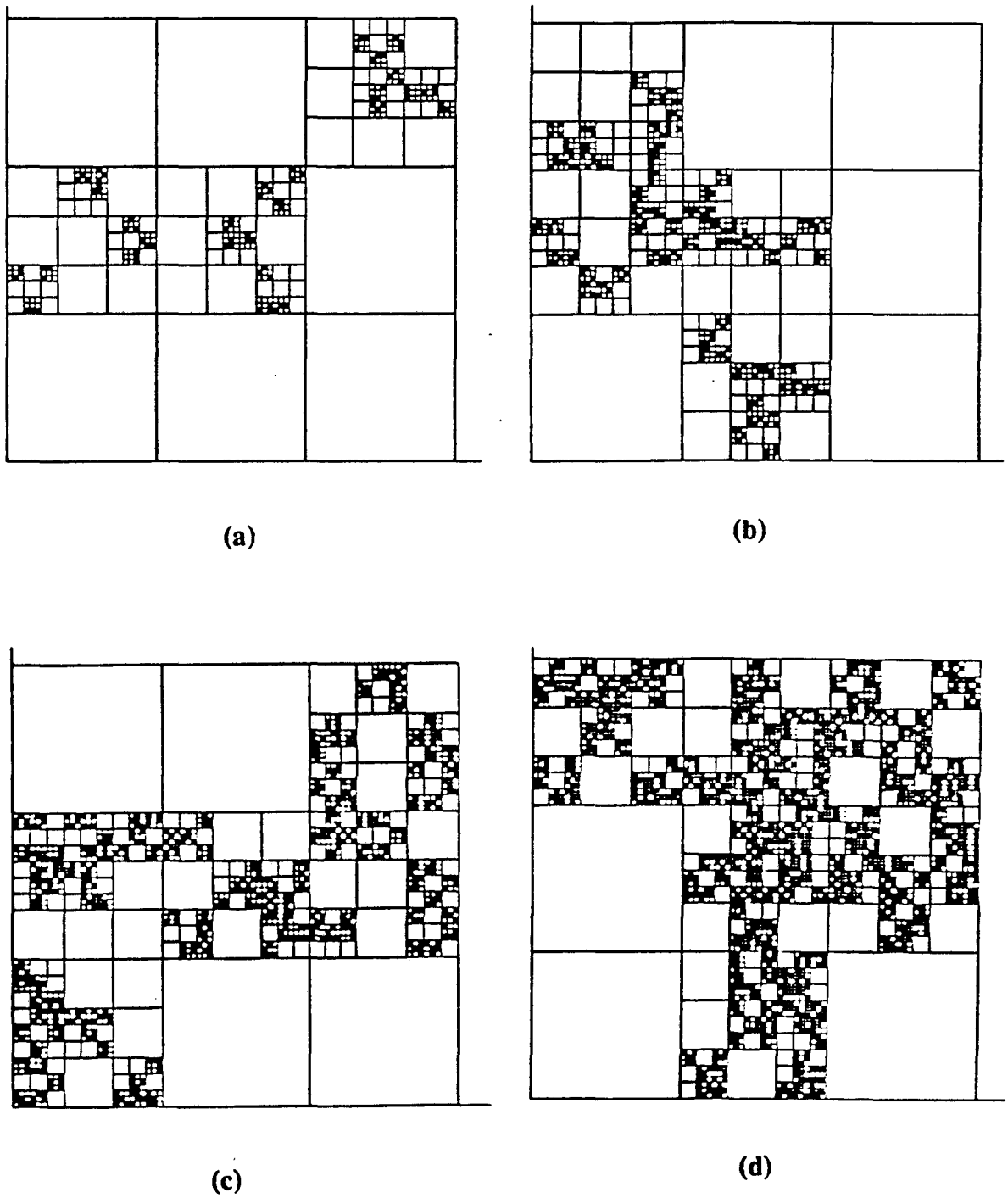


**Figure 5.8** Modified Sierpinski carpets with fractures placed at random (a) $N = 3$, (b) $N = 4$, (c) $N = 5$, and (d) $N = 6$.

where $D$ is the fractal dimension and $L$ is a constant which depends on the lacunarity of the fractal structure. Lacunarity is described in Mandelbrot (1983) and has to do with the "texture" of a fractal structure. The volume of a sphere is given by

$$V(r) = \frac{4}{3}\pi r^3 = Cr^d \tag{5.6}$$

where $C$ is a geometric constant and $d$ is the Euclidean dimension. The fractal density, in three dimensions, is the ratio of the fractal mass within a sphere to the volume of that sphere. The fractals created for this study represented fractures, so the fractal density in this case is also the fracture density. The fracture density for a two dimensional rock system is shown in Equation 5.7 to be the ratio of the number of fractures within a circle, to the area of that circle.

$$\rho(r) = \frac{N(r)}{A(r)} = \frac{Lr^D}{Cr^d} \propto r^{D-d} \tag{5.7}$$

where

$\rho(r)$ = fracture density $\quad N(r)$ = number of fractures

$A(r)$ = area of a circle $\quad r$ = radius

For the area of a circle the Euclidean dimension equals two and Equation 5.7 can be written as:

$$\rho(r) \propto r^{D-2} \tag{5.8}$$

The method used to calculate the fractal dimension was described by Orbach (1982) and is explained below. First, an origin is chosen within the rock system, from which the fracture density calculations will be made. Next, concentric circles are drawn around the origin. The number of fractures contained within each circle is counted and the fracture density for that radius is calculated. The density as a function of radius is plotted on log-log paper. The slope of this line will be

$D - 2$, as seen from Equation 5.8, which leads to a direct measure of the fractal dimension. As mentioned by Orbach (1982), and observed during this study, there were large fluctuations in the slope of the fracture density lines. The fluctuation in density is a measure of the lacunarity of the fractal. A number of fracture density calculations, from different origins, were made in order to find an average fractal dimension for the network.

The fracture density plots of the eight percolating lattice networks used in this study are shown in Figures 5.9 and 5.10. The thin lines represent the fracture densities calculated from different origins within the network. The number of origins chosen varied from four to seven. The average slope of the straight line portion of these thin lines is represented by the thick line. Less weight is given to the fracture density values at larger radii in case they were affected by the boundaries of the system. Only the radii within the range $a \leq r \leq \xi_p$ were used for calculating the fracture density. The slope of the thick lines gives an average backbone fractal dimension for each of the percolating rock systems.

For the modified carpet meshes the fracture density calculations were only done from the centrally located origin. An average backbone fractal dimension was found for each value of $N$ from the seven meshes generated at that $N$. The fracture density plots at the four values of $N$ used in this study are pictured in Figure 5.11. The thin lines are the fracture densities of the seven different meshes at each $N$. The slope of the thick lines gives an average backbone fractal dimension for a modified carpet at that value of $N$.

### 5.6. Radial Fractal Dimension

Using the fracture density method, another fractal dimension was calculated for both types of rock systems. This fractal dimension is called the radial fractal dimension. It was calculated by counting only the radial components of the

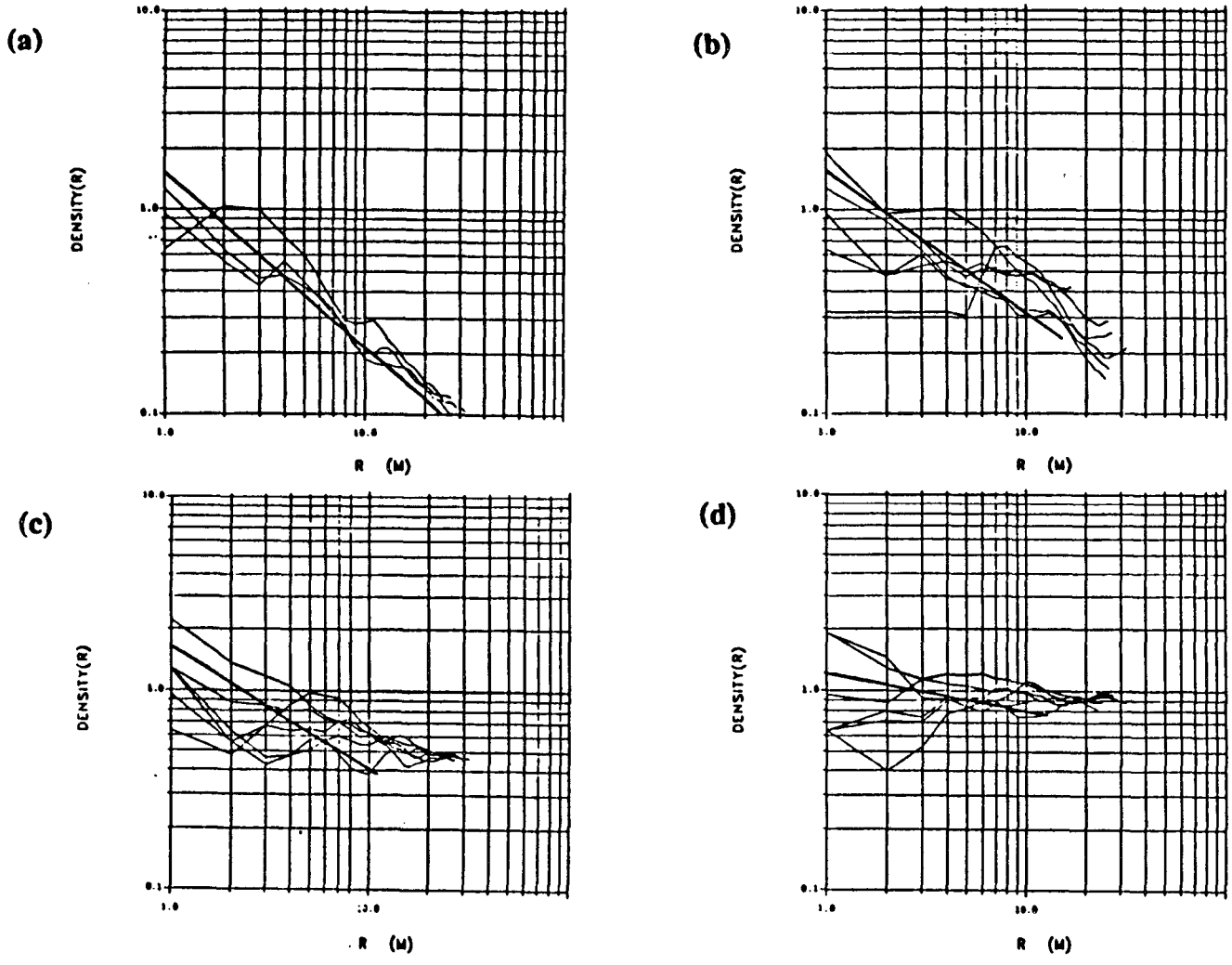


**Figure 5.9** Fracture density plots of the size 64 percolating networks (a) $p = 0.3473$, $D = 1.2$ (b) $p = 0.3450$, $D = 1.3$ (c) $p = 0.3500$, $D = 1.4$ (d) $p = 0.4000$, $D = 1.8$.

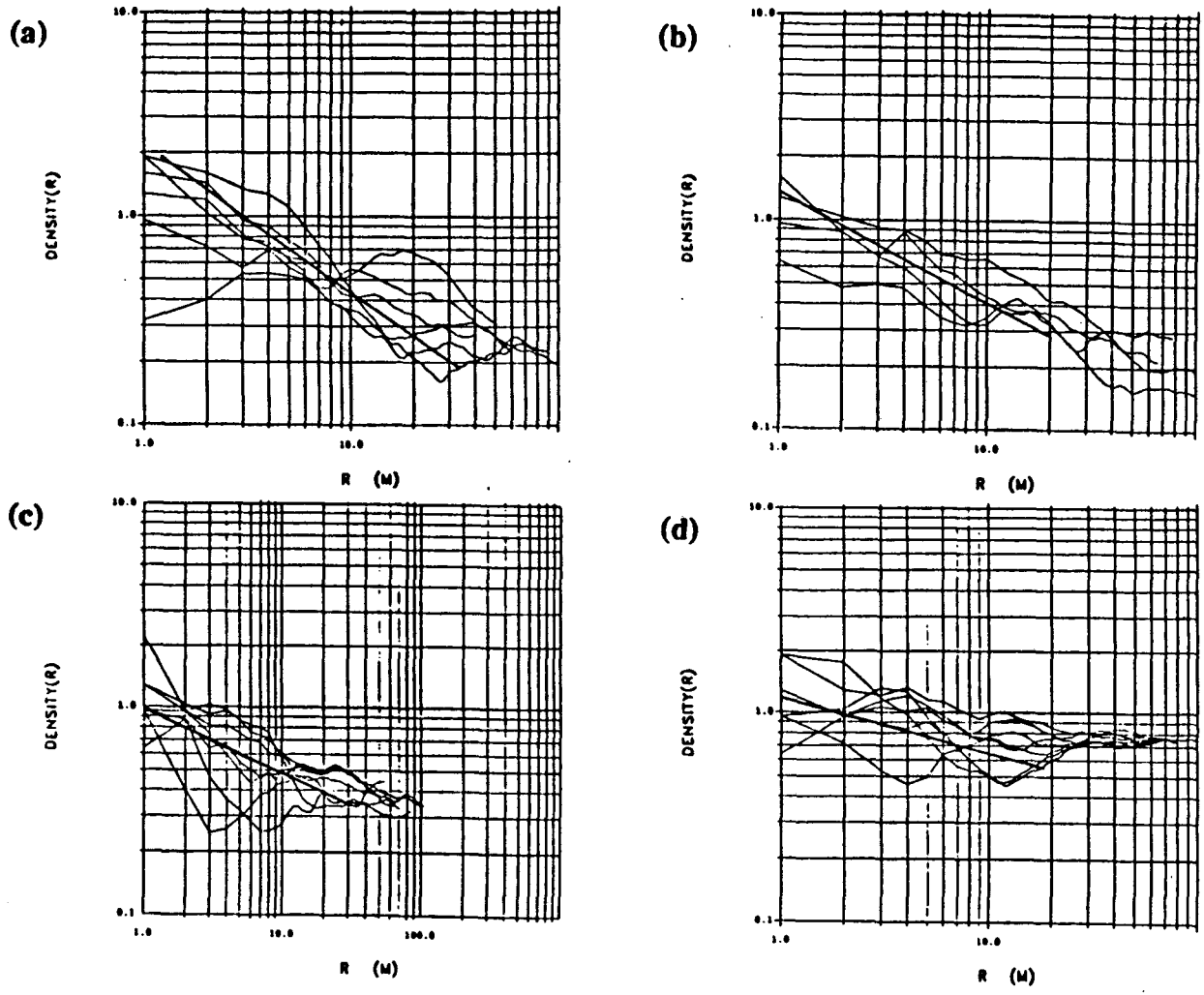


**Figure 5.10** Fracture density plots of the size 243 percolating networks (a) $p = 0.3473$, $D = 1.3$ (b) $p = 0.3450$, $D = 1.5$ (c) $p = 0.3500$, $D = 1.7$ (d) $p = 0.3800$, $D = 1.7$.

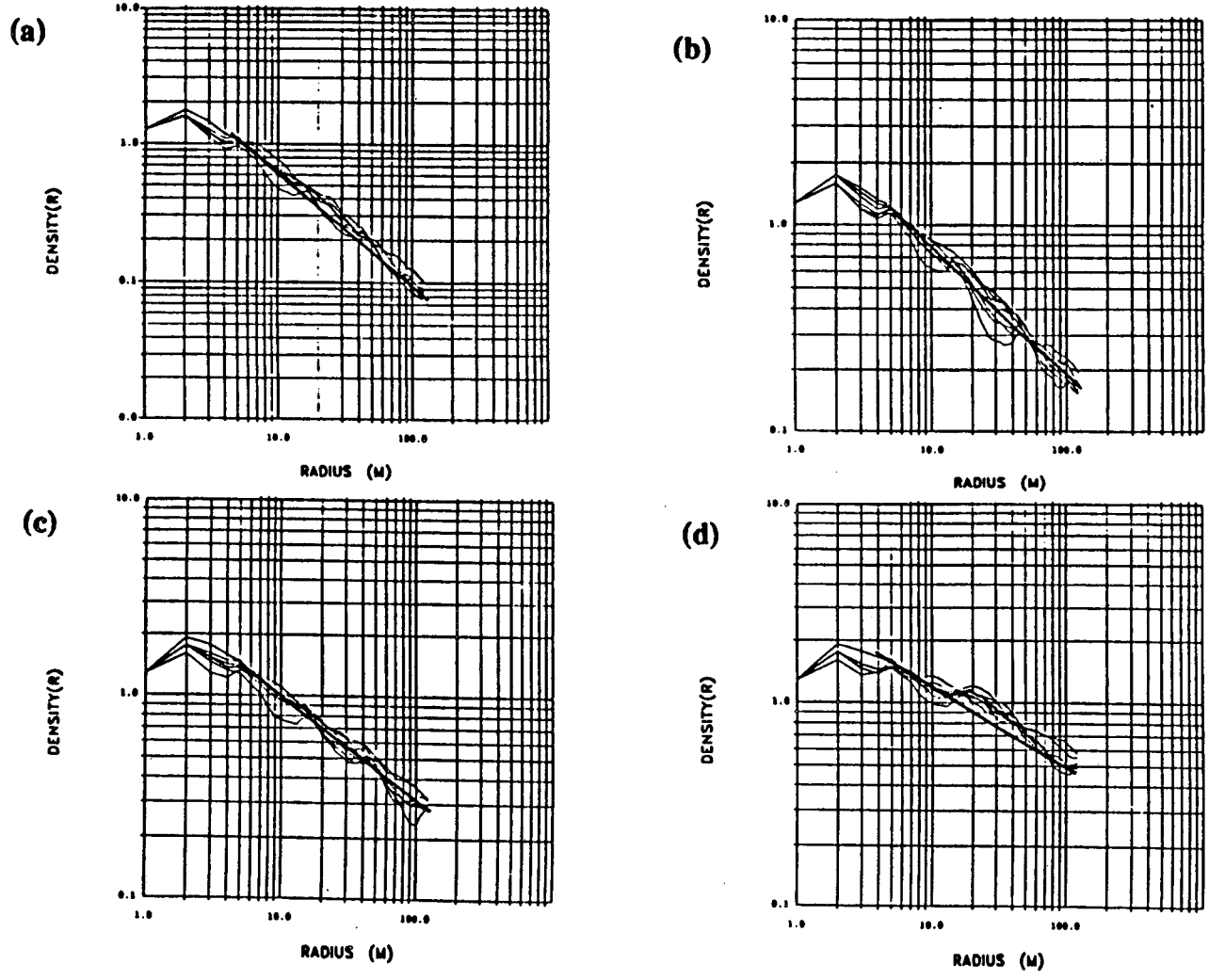


**Figure 5.11** Fracture density plots of the modified Sierpinski carpets (a) $N = 3$, $D = 1.2$ (b) $N = 4$, $D = 1.4$ (c) $N = 5$, $D = 1.5$ (d) $N = 6$, $D = 1.6$.

fracture rather than the whole fracture. The radial component is the portion of the fracture that can be projected onto any ray emanating from the chosen orgin. It was expected that this dimension, rather than the backbone fractal dimension, would better describe the physical processes occuring during a well test. During the well test the pressure changes caused by the flowing fluid are monitored. The pressure front is not affected by the tortuous flow paths inherent in the fractured rock system. At a given time step, the pressure within a fracture will be equal at a given straight line distance from the well. This is true throughout the mesh, since the dead end fractures have been removed. When calculating the radial fractal dimension some of the fracture's tortuosity is simplified in the attempt to find a geometric factor that describes this pressure behavior. Figures 5.12, 5.13 and 5.14 show the radial fracture density plots for the small and large percolating networks and the modified carpet meshes, respectively.

### 5.7. Flow Equation Solution

The backbone and radial fractal dimensions take into account all fractures appearing in the rock system and were calculated in order to compare them with the dimension of the actual fracture flow system. A fracture flow system is defined to be a system that consists of only the fractures that contribute to flow. The dimension that describes such a system will be called the flow dimension, $n$. This flow dimension is a non-Euclidean dimension, meaning that its values are not constrained to being integers. This means that the flow dimension can be found for a rock system of any configuration.

John Barker (Barker 1988) solved the flow behavior of fluid during a well test analytically, and his generalized solution can be used to calculate the flow dimension for any rock system. This generalized solution for a constant flow rate well test with an infinitesimal source and infinite flow region is:

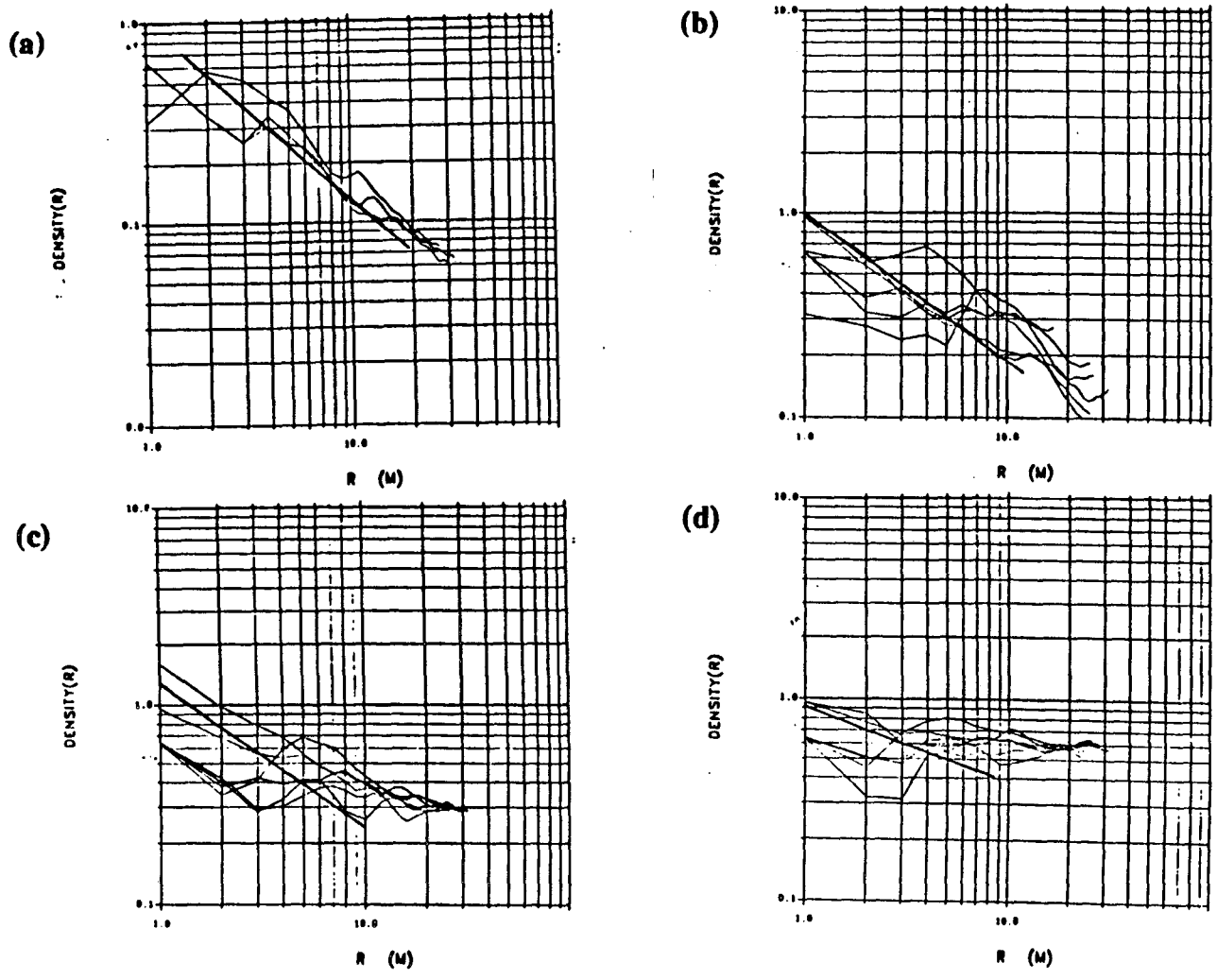


**Figure 5.12** Radial fracture density plots of the size 64 percolating networks (a) $p = 0.3473$, $D = 1.1$ (b) $p = 0.3450$, $D = 1.3$ (c) $p = 0.3500$, $D = 1.3$ (d) $p = 0.4000$, $D = 1.6$.

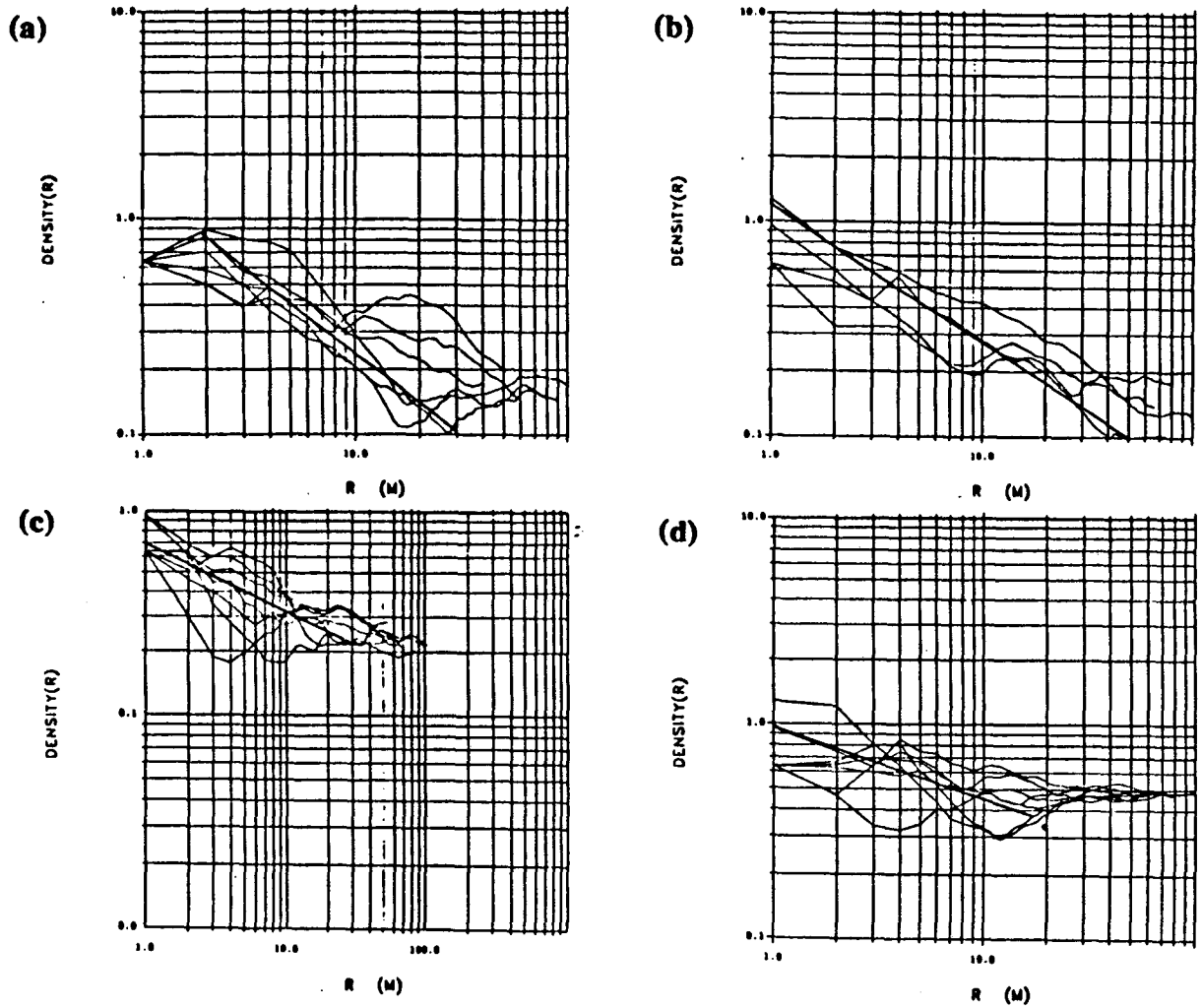


**Figure 5.13** Radial fracture density plots of the size 243 percolating networks (a) $p = 0.3473$, $D = 1.3$ (b) $p = 0.3450$, $D = 1.4$ (c) $p = 0.3500$, $D = 1.7$ (d) $p = 0.3800$ $D = 1.7$.

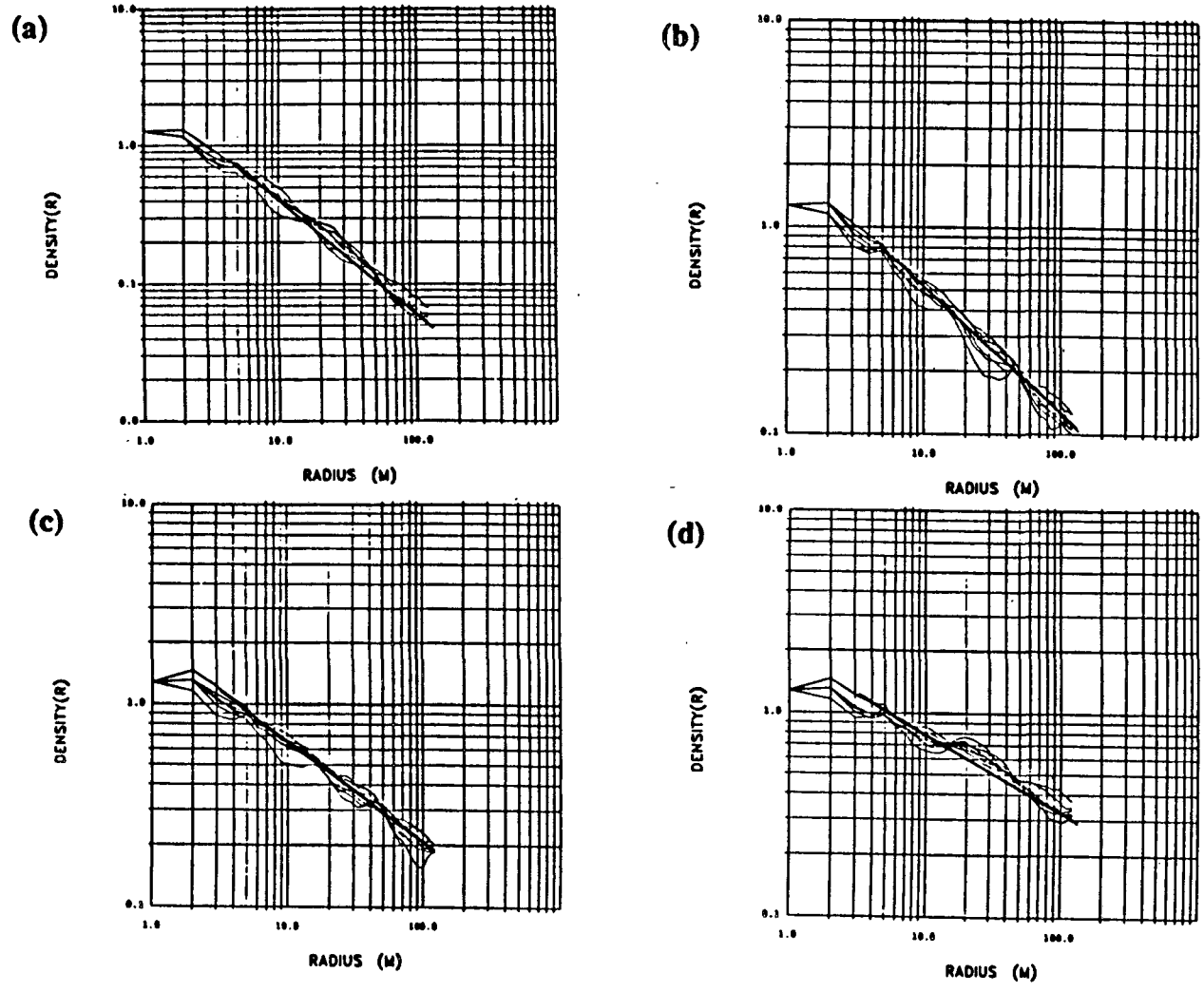


**Figure 5.14** Radial fracture density plots of the modified Sierpinski carpets (a) $N = 3$, $D = 1.2$ (b) $N = 4$, $D = 1.4$ (c) $N = 5$, $D = 1.5$ (d) $N = 6$, $D = 1.6$.

$$h(r,t) = \frac{Q_0 r^{2\nu}}{4\pi^{1-\nu} K_f b^{3-n} \nu} \Gamma(-\nu, u) \qquad (\nu < 1) \qquad (5.9)$$

The definition of the variables is as follows:

$h$ = head

$r$ = radial distance from the source when measured along the flow path

$t$ = time

$Q_0$ = constant volumetric flowrate

$\nu = 1 - \frac{n}{2}$

$n$ = flow dimension (dimension of the fracture flow system)

$K_f$ = hydraulic conductivity of the fractured rock system

$b$ = extent of flow region

$\Gamma(1-\nu)$ = (complementary) incomplete gamma function

$u = \frac{S_{sf} r^2}{4K_f t}$

$S_{sf}$ = specific storage of the fractured rock system

The log-log plot of the incomplete gamma function, $\Gamma(-\nu, u)$, as a function of $u$ is shown in Figure 5.15. The curves tend to straight lines as $u$ decreases, which relate to an increasing time. To study this behavior let us look at the asymptotic form of the head expression.

$$h(r,t) = \frac{Q_0}{4\pi^{1-\nu} K_f b^{3-n} \nu} \left[ \left[ \frac{4K_f t}{S_{sf}} \right]^{\nu} - \Gamma(1-\nu) r^{2\nu} \right] \qquad (\nu \neq 0) \qquad (5.10)$$

It is pointed out by Barker that the time dependent term, $\left[ \frac{4K_f t}{S_{sf}} \right]^{\nu}$, dominates for large times when $n$ is less than two. Not only does this explain the linear portion of the lines in Figure 5.15, but also shows that the straight portion will have a slope equal to $\nu$. This is an important relationship that results in a direct measure

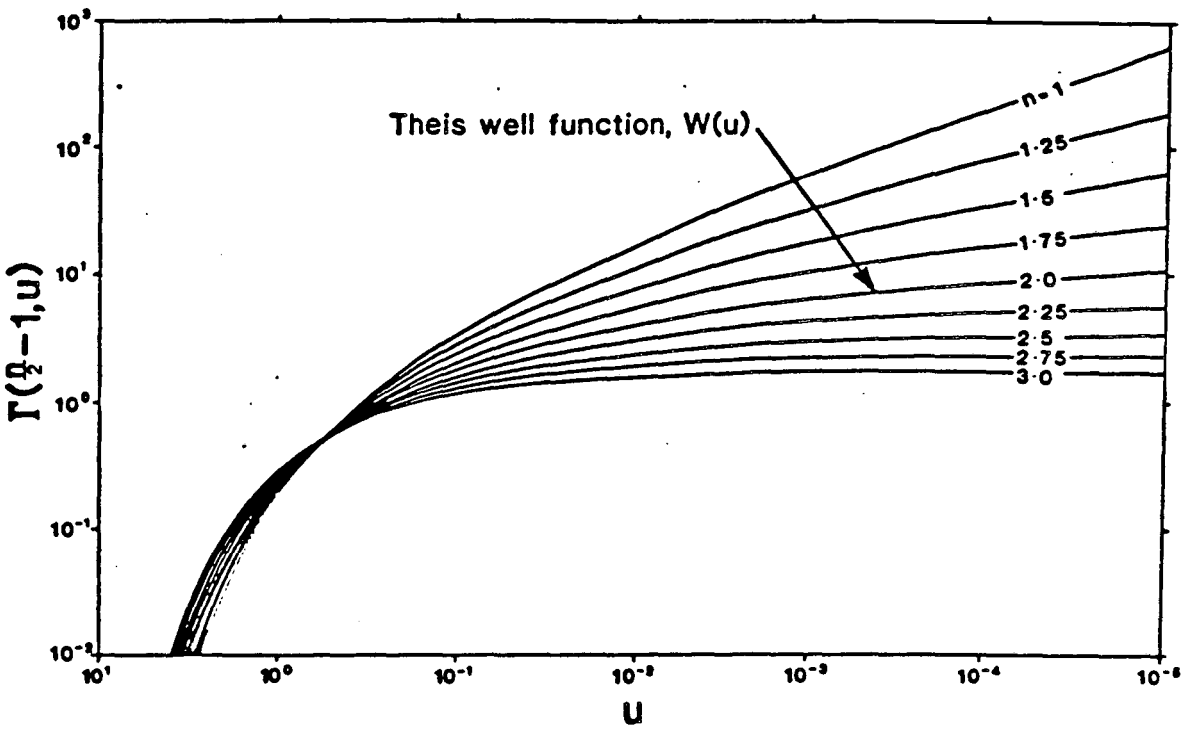


**Figure 5.15** Incomplete gamma function (Barker 1988).

of the flow dimension, $n$. When the flow dimension of a system has a value less than two, the pressure response curve will asymptote to a straight line of slope equal to $1 - \frac{n}{2}$. Therefore, by using the data from well tests on any rock system to obtain a pressure response curve, the flow dimension can be found for that rock system.

For the constant flow rate well tests modeled in this study the head values at various times were recorded and plotted on a log-log plot. The pressure response curves had a straight line portion whose slope was equal to $\nu$. Figures 5.16, 5.17 and 5.18 show the pressure response curves for the small and large percolating networks and the modified carpet meshes, respectively. The flow dimension was solved for, $n = 2 - 2\nu$. The flow dimension of each mesh was compared with the two fractal dimensions of that mesh.

## 5.8. Results

The values of both the backbone and radial fractal dimensions and the flow dimensions of the eight percolating fracture networks are shown in Tables 5.1 and 5.2. The probabilities range from 34.5% to 40% and result in fractal dimensions between one and two. The probability $p$ and the two fractal dimenstions are not uniquely related, which is expected since the networks were created from finite lattices. The relationship between the three different dimensions, rather than the numbers themselves, is important here. The flow dimension always has the lowest value. Of the backbone and radial fractal dimensions, the radial fractal dimension is always closer to the flow dimension. The radial fractal dimension is a better approximation because its calculation is less affected by the tortuous flow paths of the rock system than is the backbone fractal dimension.

Table 5.3 shows the results from the four modified Sierpinski carpet

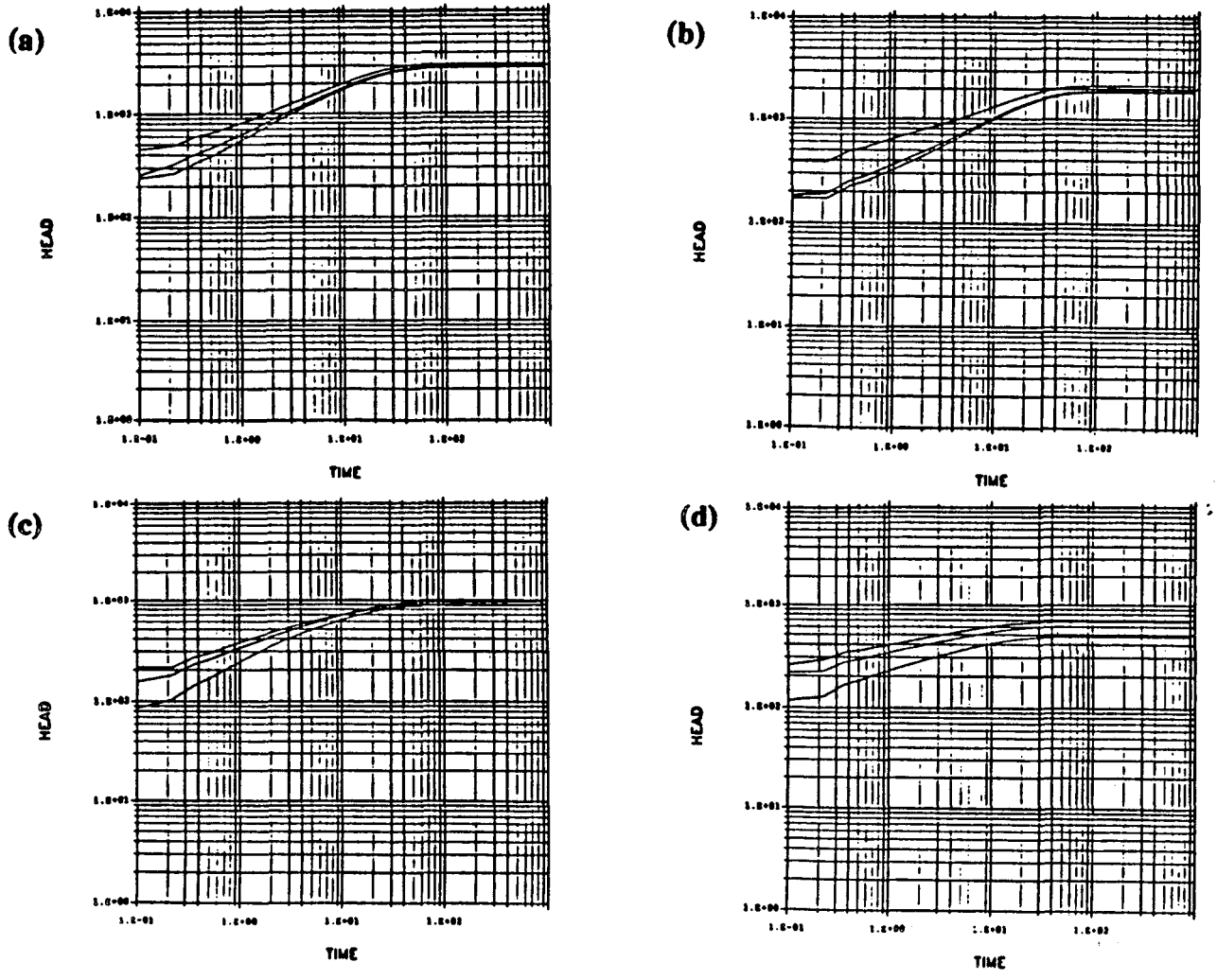


**Figure 5.16** Pressure response curves of the size 64 percolating networks (a) $p = 0.3473$, (b) $p = 0.3450$, (c) $p = 0.3500$, and (d) $p = 0.4000$.

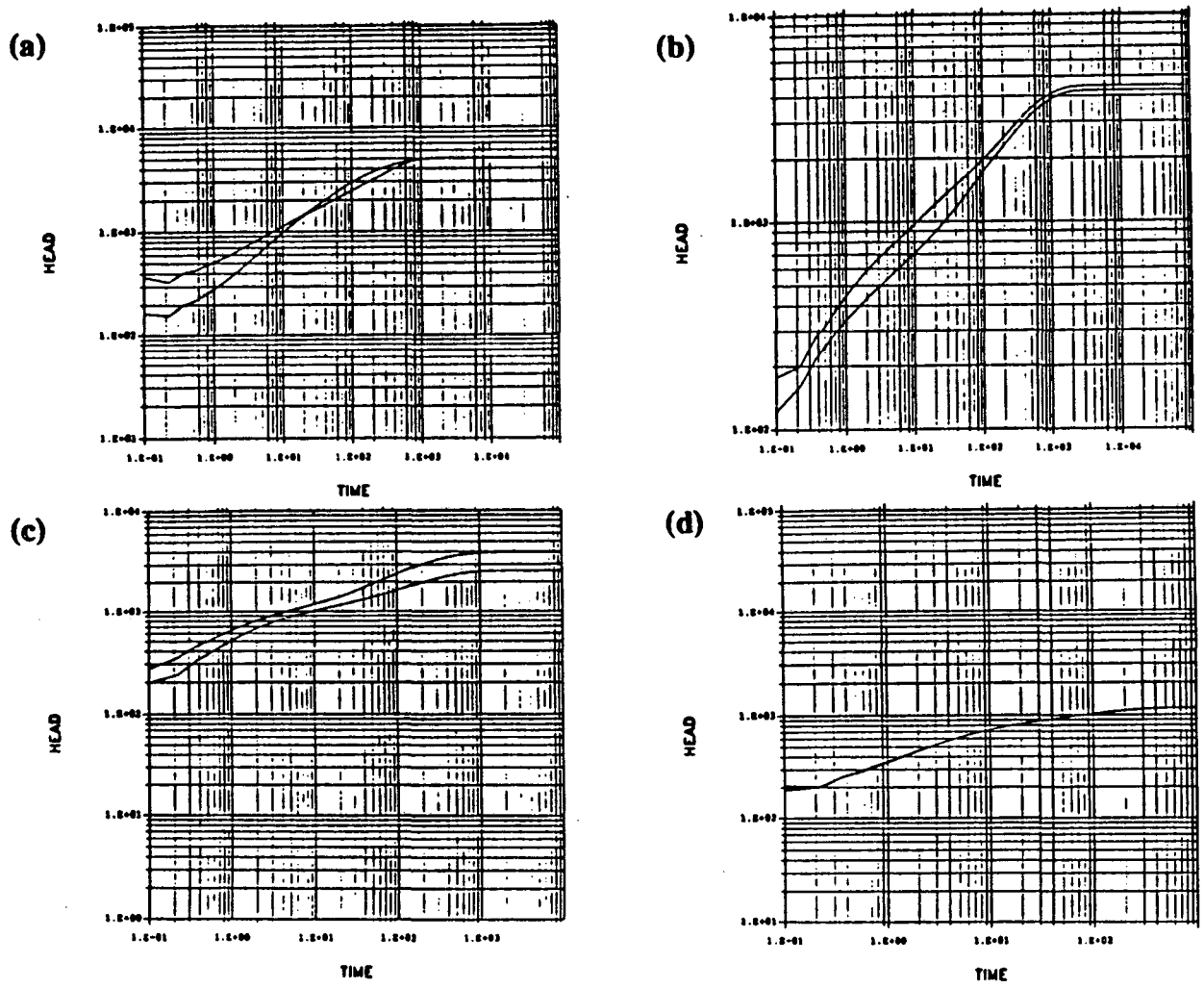


**Figure 5.17** Pressure response curves of the size 243 percolating networks (a) $p = 0.3473$, (b) $p = 0.3450$, (c) $p = 0.3500$, and (d) $p = 0.3800$.

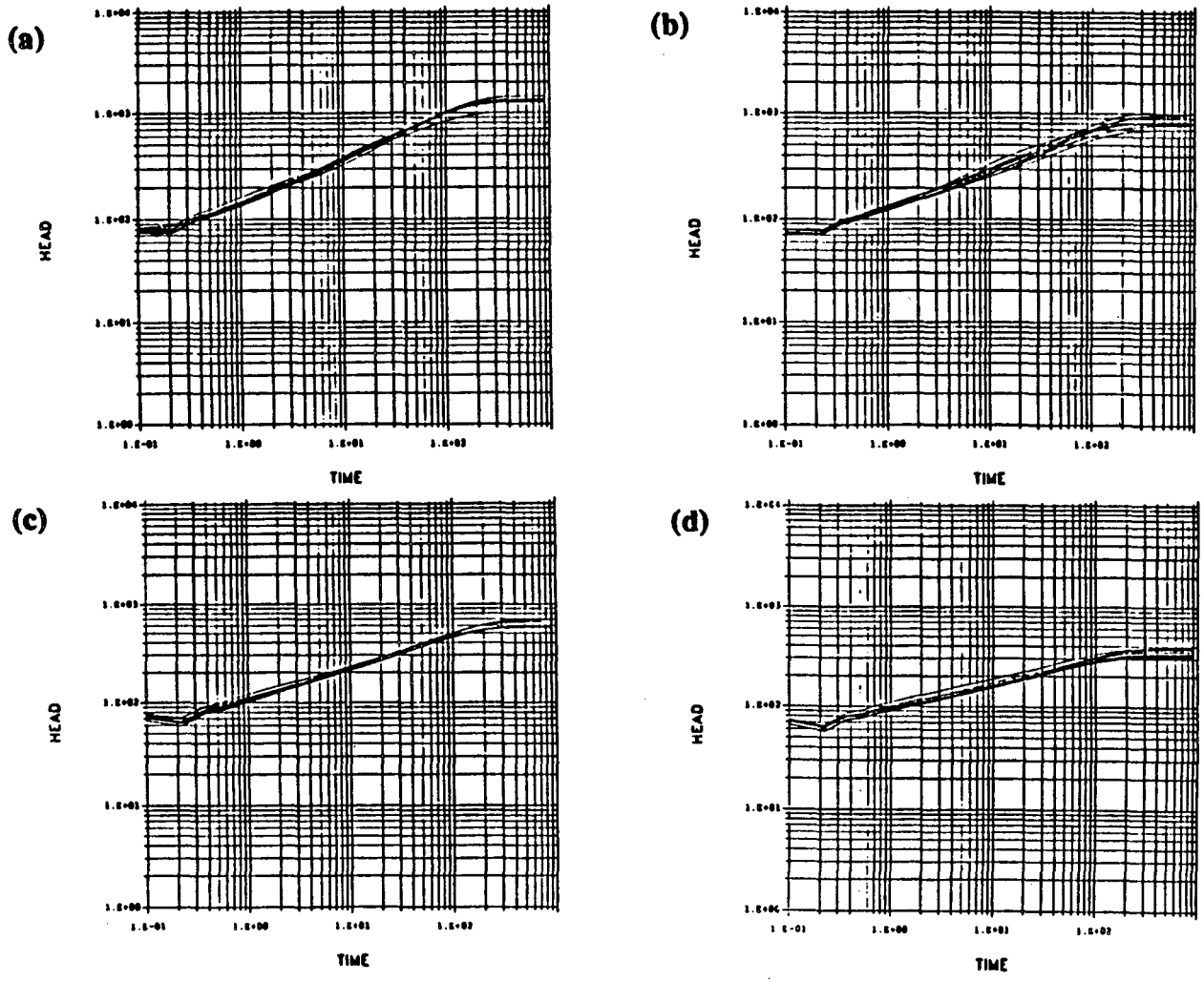


**Figure 5.18** Pressure response curves of the modified Sierpinski carpets (a) $N = 3$, (b) $N = 4$, (c) $N = 5$, and (d) $N = 6$.

**Table 5.1**
Geometric and flow dimensions of the size 64 percolating networks.

| p<br>Fraction Filled | D<br>Backbone Fractal Dimension | $D_R$<br>Radial Fractal Dimension | n<br>Flow Dimension |
|---|---|---|---|
| 0.3450 | 1.3 | 1.3 | 1.2 |
| 0.3473 | 1.2 | 1.1 | 1.1 |
| 0.3500 | 1.4 | 1.3 | 1.3 |
| 0.4000 | 1.8 | 1.6 | 1.6 |

**Table 5.2**
Geometric and flow dimensions of the size 243 percolating networks.

| p<br>Fraction Filled | D<br>Backbone Fractal Dimension | $D_R$<br>Radial Fractal Dimension | n<br>Flow Dimension |
|---|---|---|---|
| 0.3450 | 1.5 | 1.4 | 1.3 |
| 0.3473 | 1.3 | 1.3 | 1.1 |
| 0.3500 | 1.7 | 1.7 | 1.6 |
| 0.3800 | 1.7 | 1.7 | 1.7 |

**Table 5.3**
Geometric and flow dimensions of the modified Sierpinski carpets.

| N<br>Number Of Fractured Squares | D<br>Backbone Fractal Dimension | $D_R$<br>Radial Fractal Dimension | n<br>Flow Dimension |
|---|---|---|---|
| 3 | 1.2 | 1.2 | 1.2 |
| 4 | 1.4 | 1.4 | 1.3 |
| 5 | 1.5 | 1.5 | 1.4 |
| 6 | 1.6 | 1.6 | 1.5 |

rock systems. The number of squares fractured within a carpet varied from three to six and resulted in fractal dimensions between one and two. It may be observed that the trend of the dimensions is the same for the modified Sierpinski carpets as it was for the percolating networks. That is, the two geometrically calculted fractal dimensions are always larger than the flow dimension. However, there is not a great difference between the radial fractal dimension and the backbone fractal dimension due to the systematic structure of the carpet.

## 5.9. Conclusions

There have been three major points learned from this study. The first point deals with the difference between the geometrical fractal dimensions and the flow dimensions. The geometrical fractal dimensions, namely the backbone fractal dimension and the radial fractal dimension, describe the structure of the rock system as a whole. Every fracture within the system is taken into account when calculating these dimensions. The flow dimension, however, describes only the part of system that is seen by the flowing fluid. The flowing fluid does not necessarily flow through every fracture in the system. Due to the selective behavior of the flowing fluid, the flow dimension, $n$, is always less than or equal to the geometrical fractal dimensions. The second point concerns the calculation of the flow dimension. The flow dimension is found from the pressure response curve of the fluid during a well test. The shape of the pressure response curve is dictated by the hydraulic behavior of the rock. Therefore the flow dimension, $n$, reflects the hydraulic behavior of the rock. Lastly, and most importantly, the practical significance of the flow dimension, $n$, must be emphasized. In this study it was shown that the geometric dimension of a fracture system does not necessarily reflect the flow dimension of the fracture system. Therefore, when analyzing flow through any fracture system the flow dimension, $n$, should be used to characterize

the flow behavior of that fractured rock system.

# CHAPTER 6

# CONCLUSIONS AND FUTURE STUDIES

The main purpose of this paper was to study the hydraulic behavior of various hierarchical rock geometries. The dependence of the flow on the rock geometry was shown in two distinctly different studies. The first of these studies was presented in Chapter 4 and concerned the dependence of permeability on the fracture length and aperture. The permeabilities of the systems were found to depend on the fracture lengths. The degree of this dependence was shown to be a function of the aperture distribution. For every aperture distribution, however, the pattern of the permeability versus fracture length curves was similar. The curves were initially flat, indicating a constant permeability, while the first six or seven fracture length sets were removed. The curves then had sudden drops in permeability when the systems contained only the longer fractures, which constitute 20% or less of the original number of fractures. This result indicates a cutoff length when the fractures need to be explicitly modeled. For this study the cutoff length was about 1/4 of the length of the flow region being modeled. Modeling just the fractures at or above the cutoff length was sufficient to achieve a representation of the overall flow properties of the system.

The three different aperture distributions used had varying affects on the permeability. The constant aperture distribution caused the permeability to be less affected by the fracture geometry since all the fractures had an equal aperture. The permeability was essentially the same for three different fracture arrangements. For the constant aperture distribution the permeability is mostly dependent on the last two fracture length sets (3.2 m to 6.4 m and 6.4 m to 12.8 m). The correlated aperture distribution resulted in rock systems with the highest permea-

bility of all the systems studied. The permeabilties of the systems with correlated distributions were affected by the fracture geometry. These effects are seen by a range in permeabilities for the three realizations presented. The permeability of these systems depended mostly on the longest fracture set (6.4 m to 12.8 m). The distributed aperture distribution resulted in permeability effects that were a mixture of the results from the other two distributions. The systems with distributed apertures had ranges in permeabilities as did the correlated aperture systems. However, for the distributed systems, the permeability's dependence on the fracture length was similar to that observed for the constant aperture systems.

Explicitly modeling only the larger fractures (6.4 m to 12.8 m) and replacing the smaller fractures with an equivalent porous media resulted in a fracture-matrix system with the same overall hydraulic properties at steady-state conditions as the fracture only system. For the transient time period the fracture-matrix system was not found to be equivalent to the fracture only system. The porous media cannot replicate local heterogeneities caused by the small fractures.

The validity of using porous media in place of small fractures is scale dependent. If the area of interest is within the system, substitution of the small fractures by porous media may not be valid. If the concern of the study is on a scale the size of the system then the substitution seems valid. These conclusions are made from the results of this study and more work needs to be done to substantiate them.

This study was only a starting point to the understanding of the dependence of permeability on the fracture length and aperture. Future studies could be done with different values of fracture density. The role of the larger fractures may change with an increase or decrease in the fracture density. A method of calculating this cutoff length is presented in Hestir and Long (1990). The substitution of small fractures by porous media could be done with the distributed and correlated

aperture distributions. Mass transport should be modeled on the fracture only meshes and the fracture-matrix meshes that are both constructed with various aperture distributions. Mass transport is dictated by flow paths available for flow. The substitution of porous media for small fractures may alter those flow paths and give different results than the fracture only mesh. The dependence of the aperture distribution on the flow paths used could also be studied from this modeling.

The flowing fluids choice of paths was indirectly examined in the second study, presented in Chapter 5. This examination was done by calculating the dimension of the flow system from a pressure response curve. The resulting flow dimensions were observed to be always less than or equal to any geometrically calcualted dimensions of the fracture systems. The flow dimension was shown to reflect the hydraulic behavior of the rock system. Most importantly, it was found that the flow dimension could be used to characterize the flow behavior of a fracture rock system.

Finding an exact relationship between the flow dimension and the geometric dimensions would be useful in future work on modeling fractured rock. The radial fractal dimension was a first attempt at calculating the flow dimension from the geometry of the fracture system. The method for calculating the radial fractal dimension could be refined in future studies. The effects of the fracture tortuosity on the calculation of the radial fractal dimension should be minimized. Another approach for finding a connection is to give more weight to fractures constituting the direct flow paths than the fractures on circuitous flow paths.

In addition to finding a connection between the flow dimension and geometric dimension work should also be done with field well test data. Flow dimensions calculated from field pressure response curves could be matched with flow dimensions from fracture systems. The geometry of the matched fracture

system would be a first approximation of the field flow geometry. Comparisons with field data may necessitate modeling in three dimensions.

# REFERENCES


Adler, P.M. (1985). Transport processes in fractals. VI. Stokes flow through Sierpinski carpets. Phys. Fluids, v.29, n.1, p.15-22.

Baecher, G.B., N.A. Lanney and H.H. Einstein. (1977). Statistical Description of Rock Properties and Sampling. Proceedings of the 18$^{th}$ U.S. Symposium on Rock Mechanics, 5C1-8.

Baecher, G.B. and N.A. Lanney. (1978). Trace Length Biases in Joint Surveys. Proceedings of the 19$^{th}$ U.S. Symposium on Rock Mechanics, v.1 p.56-65.

Barenblatt, G.I., Iu.P. Zheltov and I.N. Kochina. (1960). Basic Concepts in the Theory of Seepage of Homogeneous Liquids in Fissured Rocks. J. Appl. Math. Mech., v.24, n.5, p.1286-1303.

Barker, J.A. (1988). A Generalized Radial Flow Model for Hydraulic Tests in Fractured Rock. Water Resources Research, v.24, n.10, p.1796-1804.

Barton, C.C., T.A. Schutter, W.R. Page and J.K. Samuel. (1987). Transactions of American Geophysical Union, v.68, n.44.

Barton, C.M. (1978). Analysis of Joint Traces. Proceedings of the 19$^{th}$ U.S. Symposium on Rock Mechanics, American Institute of Mining Engineers, p.39-40.

Bear, J. (1972). Dynamics of Fluids in Porous Media. Elsevier, New York.

Billaux, D., S. Bodea and J. Long. (1988). FMG, RENUM, LINEL, ELLFMG, ELLP and DIMES: Chain of Programs for Calculating and Analyzing Fluid Flow through Two-Dimensional Fracture Networks- Theory and Design. Lawrence Berkeley Laboratory Report, LBL-24914.

Bodvarsson, G.S. (1982). Mathmatical Modeling of the Behavior of Geothermal Systems Under Exploitation. Ph.D. Thesis, University of California at Berkeley.

Bodvarsson, G.S. and C.F. Tsang. (1982). Injection and Thermal Breakthrough in Fractured Geothermal Reservoirs. J. of Geophysical Research, v.87, n.B2, p.1031-1048.

Chen, D.C. and D. Wilkinson. (1985). Pore-Scale Viscous Fingering in Porous Media. Physics Review Letters, v.55, n.18, p.1892-1895.

Dershowitz, W.S. and H.H. Einstein. (1988). Characterizing Rock Joint Geometry with Joint System Models. Rock Mechanics and Rock Engineering, v.21, n.1, p.21-51.

de Swaan, O.A. (1976). Analytical Solutions for Determining Naturally Fractured Reservoir Properties by Well Testing. Society of Petroleum Engineers Journal, AIME, p.112-122.

Englman, R., Y. Gur and Z. Jaeger. (1983). Fluid Flow Through a Crack Network in Rocks. Journal of Applied Mechanics, v.50, p.707-711.

Feder, J. (1988). Fractals. Plenum Press, New York.

Gilmour, P., D. Billaux and J.C.S. Long. (1986). Models for Calculating Fluid Flow in Randomly Generated Three-Dimensional Networks of Disc Shaped Fractures- Theory and Design of FMG3D, DISCEL and DIMES. Lawrence Berkeley Laboratory Report, LBL-19515.

Hestir, K. and J. Long. (1990). Analytical Expressions for the Permeability of Random Two-Dimensional Poisson Fracture Networks Based on Percolation and Equivalent Media Theories. Submitted to Journal of Geophysical Research.

Hewett, T.A. (1986). Fractal Distributions of Reservoir Heterogeneity and Their Influence on Fluid Transport. Society of Petroleum Engineers Report, SPE-15386.

Hudson, J.A. and S.D. Priest. (1979). Discontinuities and Rock Mass Geometry. International Journal of Rock Mechanics, Mineral Science and Geomechanics, Abstracts, v.16, p339-362.

Karasaki, K. (1987). Well Test Analysis in Fractured Media. Ph.D. Thesis, University of California at Berkeley.

Kazemi, H. (1969). Pressure Transient Analysis of Naturally Fractured Reservoirs with Uniform Fracture Distribution. Society of Petroleum Engineers Journal, AIME, v.B246, p.451-462.

Lai, C.H. (1985). Mathmatical Models of Thermal and Chemical Transport in Geologic Media. Ph.D. Thesis, University of California at Berkeley.

Long, J.C.S., J.S. Remer, C.R. Wilson and P.A. Witherspoon. (1982). Porous Media Equivalents for Networks of Discontinuous Fractures. Water Resources Research, v.18, n.3, p.645-658.

Long, J.C.S. (1983). Investigation of Equivalent Porous Medium Permeability in Networks of Discontinuous Fractures. Ph.D. Thesis, University of California at Berkeley.

Long, J.C.S. and P.A. Witherspoon. (1985). The Relationship of the Degree of Interconnection to Permeability in Fracture Networks. Journal of Geophysical Research, v.90, n.B4, p.3087-3098.

Maloy, K.J., F. Boger, J. Feder and T. Jossang. (1987). Dynamics of Viscous-Fingering Fractals in Porous Media. Physical Review A, v.36, n.1, p.318-324.

Mandelbrot, B.B. (1982). The Fractal Geometry of Nature. W.H. Freeman, San Francisco.

Marcus, H. and D.E. Evanson. (1962). Directional Permeability in Anisotropic Porous Media. Water Resources Center Contribution n.31, University of California at Berkeley.

Marcus, H. (1962). The Permeability of a Sample of an Anisotropic Porous Medium. Journal of Geophysical Research, v.67, p.5215-5225.

Nolte, D.D., L.J. Pyrak-Nolte and N.G.W. Cook. (1987). The Fractal Geometry of the Flow Paths in Natural Fractures in Rock and the Approach to Percolation. PAGEOPH Special Issue on Fractals in Geophysics.

Okusu, N.M., K. Karasaki, J.C.S. Long and G.S. Bodvarsson. (1989). FMMG: A Program for Discretizing Two-Dimensional Fracture/Matrix Systems. User's Manual and Listings. Lawrence Berkeley Laboratory Report, LBL-26782.

Orbach, R. (1986). Dynamics of Fractal Networks. Science, v.231, p.814-819.

Oxaal, U., M. Murat, F. Boger, A. Aharony, J. Feder and T. Jossang. (1987). Viscous Fingering on Percolation Clusters. Nature, v.329, n.6134, p.32-37.

Snow, D.T. (1965). A Parallel Plate Model of Fractured Permeable Media. Ph.D. Thesis, University of California at Berkeley.

Snow, D.T. (1969). Anisotropic Permeability of Fractured Media. Water Resources Research, v.5, n.6, p.1273-1289.

Stauffer, D. (1985). Introduction to Percolation Theory. Taylor and Francis, Philadelphia.

Streltsova, T.D. (1983). Well Pressure Behavior of a Naturally Fractured Reservoir. Society of Petroleum Engineers Journal, Oct., p.769-780.

Warren, J.F. and P.J. Root. (1963). The Behavior of Naturally Fractured Reservoirs. Society of Petroleum Engineers Journal, AIME, v.228, p.245-255.

Wilson, C.R. (1970). An Investigation of Laminar Flow in Fractured Porous Rocks. Ph.D. Thesis, University of California at Berkeley.

Witherspoon, P.A., J.C.Y. Wang, K. Iwai and J.E. Gale. (1980). Validity of Cubic Law for Fluid Flow in a Deformable Rock Fracture. Water Resources Research, v.16, p.1016-1024.

Zallen, R. (1983). The Physics of Amorphous Solids J. Wiley and Sons, New York.

LAWRENCE BERKELEY LABORATORY
TECHNICAL INFORMATION DEPARTMENT
1 CYCLOTRON ROAD
BERKELEY, CALIFORNIA 94720